PFC/JA-86-50

CLOSED ANALYTICAL MODEL OF THE ELECTRON WHISTLER AND CYCLOTRON MASER INSTABILITIES IN RELATIVISTIC PLASMA WITH ARBITRARY ENERGY ANISOTROPY

Peter H. Yoon and Ronald C. Davidson
Plasma Fusion Center
Massachusetts Institute of Technology
Cambridge, MA 02139

August, 1986

CLOSED ANALYTICAL MODEL OF THE ELECTRON WHISTLER AND CYCLOTRON MASER INSTABILITIES IN RELATIVISTIC PLASMA WITH ARBITRARY ENERGY ANISOTROPY

Peter H. Yoon and Ronald C. Davidson

Plasma Fusion Center

Massachusetts Institute of Technology, Cambridge, Massachusetts 02139

ABSTRACT

Detailed properties of the cyclotron maser and whistler instabilities in a relativistic magnetized plasma are investigated for a particular choice of anisotropic distribution function $F(p_\perp^2, p_z)$ that permits an exact analytical reduction of the dispersion relation for arbitrary energy anisotropy. The analysis assumes electromagnetic wave propagation parallel to a uniform applied magnetic field $B_0\hat{e}_z$. Moreover, the particular equilibrium distribution function considered in the present analysis assumes that all electrons move on a surface with perpendicular momentum $p_\perp = \hat{p}_\perp = \text{const.}$ and are uniformly distributed in axial momentum from $p_z = -\hat{p}_z = \text{const.}$ to $p_z = +\hat{p}_z = \text{const.}$ (so-called "waterbag" distribution in p_z). The resulting dispersion relation is solved numerically, and detailed properties of the cyclotron maser and whistler instabilities are determined over a wide range of energy anisotropy, normalized density ω_p^2/ω_c^2, and electron energy.

I. INTRODUCTION

The classical cyclotron maser[1-9] and electron whistler[6,10-13] instabilities in a uniform plasma are transverse electromagnetic instabilities[13-15] driven by an anisotropy in the average kinetic energy of the constituent electrons. These instabilities have a wide range of applicability to astrophysical and space plasmas,[3,4,8,11] to laboratory plasmas with intense RF heating,[6,7,12] and to relativistic electron beams used for microwave generation.[1,2,9] For nonrelativistic anisotropic plasma, detailed properties of the whistler instability[13] are readily calculated for a wide range of distribution functions $F(p_\perp^2, p_z)$. Here, we assume electromagnetic wave propagation parallel to a uniform applied magnetic field $B_0\hat{e}_z$, and the terms "perpendicular" and "parallel" refer to directions relative to $B_0\hat{e}_z$. For relativistic anisotropic plasma, however, because of the coupling of the perpendicular and parallel particle motions through the relativistic mass factor $\gamma = (1 + p_\perp^2/m^2c^2 + p_z^2/m^2c^2)^{\frac{1}{2}}$, properties of the cyclotron maser and whistler instabilities are usually calculated in limiting regimes which allow approximate analytical solutions or substantial simplification of the electromagnetic dispersion relation. These limiting regimes range from weak energy anisotropy, to very strong energy anisotropy, to long perturbation wavelengths, to short perturbation wavelengths.

The purpose of this paper is to investigate detailed properties of the cyclotron maser and whistler instabilities in relativistic magnetized plasma for a particular choice of anisotropic distribution function that permits an exact analytical reduction of the dispersion relation for arbitrary energy anisotropy. This calculation is intended to provide

qualitative insights regarding stability behavior for more general choices of equilibrium distribution function. The particular distribution function[15] [Eq.(7)] considered in the present analysis assumes that all electrons move on a surface with perpendicular momentum $p_\perp = \hat{p}_\perp = \text{const.}$, and are uniformly distributed in parallel momentum between $p_z = -\hat{p}_z = \text{const.}$ and $p_z = +\hat{p}_z = \text{const.}$ (so-called "waterbag" distribution in p_z). For this choice of $F(p_\perp^2, p_z)$, the integrations over $p_\perp$ and p_z in the dispersion relation [Eq. (2)] can be carried out in closed form. The resulting dispersion relation [Eq.(19)] is valid for arbitrary energy anisotropy $\hat{\beta}_\perp^2/2\hat{\beta}_z^2$ and can be used to investigate detailed stability properties over a wide range of system parameters. Here, $\hat{\beta}_\perp$ and $\hat{\beta}_z$ are defined by $\hat{\beta}_\perp = \hat{p}_\perp/\hat{\gamma}mc$ and $\hat{\beta}_z = \hat{p}_z/\hat{\gamma}mc$, where $\hat{\gamma} = (1 + \hat{p}_\perp^2/m^2c^2 + \hat{p}_z^2/m^2c^2)^{\frac{1}{2}}$.

The organization of this paper is the following. In Sec. II, we outline the theoretical model (Sec. II.A), derive the electromagnetic dispersion relation (19) for the choice of equilibrium distribution function in Eq.(7) (Sec. II.B), and (for completeness) show that Eq.(19) reduces to familiar results in the two limiting cases $\hat{\beta}_z = 0$ and $B_0 = 0$ (Sec. II.C). In Sec. III, the dispersion relation (19) is solved numerically, and detailed stability properties are investigated for both the cyclotron maser and whistler instabilities over a wide range of system parameters $\hat{\beta}_\perp^2/2\hat{\beta}_z^2$, ω_p^2/ω_c^2, $\hat{\gamma}$, and ck_z/ω_p. Here, $\omega_c = eB_0/mc$ and $\omega_p = (4\pi\hat{n}e^2/m)^{\frac{1}{2}}$ are the nonrelativistic electron cyclotron and plasma frequencies, respectively, and k_z is the axial wavenumber of the perturbation. Finally, in Sec. IV, we obtain the electromagnetic dispersion relation [Eq.(35)] for the case where the distribution in parallel momentum p_z corresponds to thermal equilibrium [Eq.(29)]. A detailed analysis of Eq.(35) will be the subject of a future investigation.

II. THEORETICAL MODEL AND DISPERSION RELATION

A. Electromagnetic Dispersion Relation

In the present analysis, we specialize to the case of stationary ions ($m_i \to \infty$) and consider a single active component of relativistic anisotropic electrons. Electromagnetic stability properties are investigated for perturbations propagating in the z-direction parallel to a uniform applied magnetic field $B_0\hat{e}_z$. Perturbations are about the class of spatially uniform equilibria with distribution function

$$f^0(\underset{\sim}{p}) = \hat{n}F(p_\perp^2, p_z) \ , \tag{1}$$

where $\hat{n}$ = const. is the ambient electron density, $p_\perp = (p_x^2 + p_y^2)^{\frac{1}{2}}$ is the particle momentum perpendicular to the magnetic field $B_0\hat{e}_z$, and p_z is the parallel momentum. The linear dispersion relation for circularly polarized electromagnetic wave perturbations propagating in the z-direction is given by

$$0 = D_T^{\pm}(\omega, k_z) = 1 - \frac{c^2k_z^2}{\omega^2} + \frac{\omega_p^2}{\omega^2}\int \frac{d^3p}{\gamma} \frac{(p_\perp/2)}{\gamma\omega - k_zp_z/m \pm \omega_c} \times \left\{\left(\gamma\omega - \frac{k_zp_z}{m}\right)\frac{\partial}{\partial p_\perp} + \frac{k_zp_\perp}{m}\frac{\partial}{\partial p_z}\right\} F(p_\perp^2, p_z) \ , \tag{2}$$

where k_z is the axial wavenumber and ω is the complex oscillation frequency with $\mathrm{Im}\omega > 0$, which corresponds to instability (temporal growth). In Eq.(2), $\omega_p^2 = 4\pi\hat{n}e^2/m$ is the nonrelativistic plasma frequency-squared; $\omega_c = eB_0/mc$ is the nonrelativistic cyclotron frequency; -e and m are the electron charge and rest mass, respectively; c is the speed of light in vacuo; $\gamma = (1 + p_\perp^2/m^2c^2 + p_z^2/m^2c^2)^{\frac{1}{2}}$ is the relativistic mass factor; the

range of integration is $\int d^3p \cdots = 2\pi \int_0^\infty dp_\perp p_\perp \int_{-\infty}^\infty dp_z \cdots$; and the normalization of F is $\int d^3p F(p_\perp^2, p_z) = 1$. Moreover, the two signs in Eq.(2) refer to electromagnetic waves with right-circular polarization (- sign) and left-circular polarization (+ sign), respectively. The dispersion relation (2) is readily extended to the case of a multicomponent plasma by making the replacements $\omega_p^2 \cdots \to \sum_j \omega_{pj}^2 \cdots$, $F(p_\perp^2, p_z) \to F_j(p_\perp^2, p_z)$, $\omega_c \to \omega_{cj}$, etc., where j labels the plasma species.

The dispersion relation (2) can be used to investigate detailed electromagnetic stability properties for a wide range of anisotropic distribution functions $F(p_\perp^2, p_z)$. For <u>relativistic</u> anisotropic plasma, we note that the perpendicular and parallel particle motions in Eq.(2) are inexorably coupled through the relativistic mass factor $\gamma = (1 + p_\perp^2/m^2c^2 + p_z^2/m^2c^2)^{\frac{1}{2}}$. For present purposes, we assume that the electrons move on a surface with constant perpendicular momentum $p_\perp = \hat{p}_\perp = \text{const}$. That is, $F(p_\perp^2, p_z)$ is assumed to have the form

$$F(p_\perp^2, p_z) = \frac{1}{2\pi p_\perp} \delta(p_\perp - \hat{p}_\perp) F_1(p_z) \ , \tag{3}$$

where $F_1(p_z)$ is the parallel momentum distribution (yet unspecified) with normalization $\int_{-\infty}^\infty dp_z F_1(p_z) = 1$. The strongly peaked distribution in $p_\perp$ in Eq.(3) can occur in laboratory plasmas when there is intense microwave heating (e.g., electron cyclotron resonance heating) of the electrons perpendicular to $B_0 \hat{e}_z$.

The integration over $p_\perp$ in Eq.(2) can be carried out in closed analytical form for the choice of distribution function in Eq.(3). Making use of $\partial\gamma/\partial p_z = p_z/\gamma m^2c^2$ and $\partial\gamma/\partial p_\perp = p_\perp/\gamma m^2c^2$, some straightforward algebra shows that Eq.(2) can be expressed as

$$0 = D_T^{\pm}(\omega,k_z) = 1 - \frac{c^2k_z^2}{\omega^2} - \frac{\omega_p^2}{\omega^2}\int_{-\infty}^{\infty}\frac{dp_z}{\gamma}F_1(p_z)$$

$$\times\left\{\frac{\gamma - k_zp_z/m\omega}{\gamma - k_zp_z/m\omega \pm \omega_c/\omega} - \frac{\hat{p}_\perp^2}{2m^2c^2}\frac{(1 - c^2k_z^2/\omega^2)}{(\gamma - k_zp_z/m\omega \pm \omega_c/\omega)^2}\right\}. \tag{4}$$

In Eq.(4), γ is defined by

$$\gamma = \left(1 + \frac{\hat{p}_\perp^2}{m^2c^2} + \frac{p_z^2}{m^2c^2}\right)^{\frac{1}{2}}, \tag{5}$$

where $p_\perp$ has been replaced by $\hat{p}_\perp$ = const.

B. Waterbag Distribution in Parallel Momentum [15]

The dispersion relation (4) can be used to investigate detailed electromagnetic stability properties for a wide range of distribution functions $F_1(p_z)$. For purposes of elucidating the essential features of the instability in relativistic anisotropic plasma, we make a particular choice of $F_1(p_z)$ for which the integrations over p_z in Eq.(4) can be carried out in closed analytical form. In particular, it is assumed that the electrons are uniformly distributed in parallel momentum between $p_z = -\hat{p}_z$ = const. and $p_z = +\hat{p}_z$ = const. That is, $F_1(p_z)$ is specified by

$$F_1(p_z) = \frac{1}{2\hat{p}_z}H(\hat{p}_z^2 - p_z^2), \tag{6}$$

where $H(x)$ is the Heaviside step function defined by $H(x) = +1$ for $x > 0$, and $H(x) = 0$ for $x < 0$. Note from Eq.(6) that $\int_{-\infty}^{\infty}dp_zF_1(p_z) = 1$. Because the electrons are uniformly distributed in parallel momentum for $|p_z| < \hat{p}_z$, we refer to the p_z-dependence of the distribution function in Eq.(6) as a

"waterbag" distribution in p_z. Combining Eqs.(3) and (6), the total distribution function $F(p_\perp^2,p_z)$ can be expressed as

$$F(p_\perp^2,p_z) = \frac{1}{2\pi p_\perp}\,\delta(p_\perp - \hat{p}_\perp)\,\frac{1}{2\hat{p}_z}\,H(\hat{p}_z^2 - p_z^2)\ . \tag{7}$$

For future reference, we first calculate the energy anisotropy associated with the distribution function in Eq.(7).

Equilibrium Properties: For the choice of distribution function in Eq.(7), it is useful to introduce the maximum energy $\hat{\gamma}mc^2$, parallel speed $c\hat{\beta}_z$, and perpendicular speed $c\hat{\beta}_\perp$ defined by

$$\hat{\beta}_z = \frac{\hat{p}_z}{\hat{\gamma}mc}\ , \qquad \hat{\beta}_\perp = \frac{\hat{p}_\perp}{\hat{\gamma}mc}\ ,$$

$$\hat{\gamma} = \left(1 + \frac{\hat{p}_\perp^2}{m^2c^2} + \frac{\hat{p}_z^2}{m^2c^2}\right)^{\frac{1}{2}} \tag{8}$$

$$= \left(1 - \hat{\beta}_\perp^2 - \hat{\beta}_z^2\right)^{-\frac{1}{2}}\ .$$

We further introduce the effective perpendicular and parallel temperatures defined by

$$T_\perp = \int d^3p\ \frac{p_\perp^2}{2\gamma m}\,F(p_\perp^2,p_z)\ ,$$

$$\frac{1}{2}\,T_z = \int d^3p\ \frac{p_z^2}{2\gamma m}\,F(p_\perp^2,p_z)\ . \tag{9}$$

Substituting Eq.(7) into Eq.(9) and carrying out the required integrations over $p_\perp$ and p_z give

$$T_\perp = \frac{1}{2}\hat{\gamma}mc^2\hat{\beta}_\perp^2 G(\hat{\beta}_z) \ ,$$

$$T_z = \frac{1}{2}\hat{\gamma}mc^2\left[1 - G(\hat{\beta}_z) + \hat{\beta}_z^2 G(\hat{\beta}_z)\right] , \tag{10}$$

where $G(\hat{\beta}_z)$ is defined by

$$G(\hat{\beta}_z) = \frac{1}{2\hat{\beta}_z}\,\ell n\left(\frac{1+\hat{\beta}_z}{1-\hat{\beta}_z}\right) \ . \tag{11}$$

From Eq.(11) and Fig. 1, we note that $G(\hat{\beta}_z)$ is a slowly increasing function of $\hat{\beta}_z$ with $G(\hat{\beta}_z) = 1 + \hat{\beta}_z^2/3\cdots$ for $\hat{\beta}_z^2 << 1$. Moreover, in the limit of a nonrelativistic plasma with $\hat{\beta}_z^2 << 1$ and $\hat{\beta}_\perp^2 << 1$, Eq.(10) reduces to the expected results, $T_\perp \to (1/2)mc^2\hat{\beta}_\perp^2$ and $T_z \to (1/3)mc^2\hat{\beta}_z^2$. Depending on the relative values of $\hat{\beta}_\perp$ and $\hat{\beta}_z$, it is clear that the choice of distribution function in Eq.(7) can cover a wide range of energy anisotropy.

Dispersion Relation: We now simplify the dispersion relation (4) for the choice of waterbag distribution $F_1(p_z)$ in Eq.(6). In this regard, it is convenient to define

$$\hat{\gamma}_\perp = \left(1 + \frac{\hat{p}_\perp^2}{m^2c^2}\right)^{\frac{1}{2}} \tag{12}$$

and rewrite the expression for $\gamma = (1 + \hat{p}_\perp^2/m^2c^2 + p_z^2/m^2c^2)^{\frac{1}{2}}$ in Eq.(5) as

$$\gamma = \hat{\gamma}_\perp\left(1 + \frac{p_z^2}{\hat{\gamma}_\perp^2 m^2c^2}\right)^{\frac{1}{2}} \ . \tag{13}$$

In the dispersion relation (4) we change variables from p_z to α where

$$p_z = (\hat{\gamma}_\perp mc)\sinh\alpha \ . \tag{14}$$

From Eqs.(13) and (14), it follows that

$$\gamma = \hat{\gamma}_\perp \cosh\alpha \ ,$$
$$\frac{dp_z}{\gamma} = mc\,d\alpha \ . \tag{15}$$

Substituting Eqs.(6), (14) and (15) into the dispersion relation (4) then gives

$$0 = D_T^{\pm}(\omega,k_z) = 1 - \frac{c^2k_z^2}{\omega^2} - \frac{\omega_p^2}{\omega^2}\frac{mc}{2\hat{p}_z}\int_{-\hat{\alpha}}^{\hat{\alpha}} d\alpha$$
$$\times \left\{ \frac{[\cosh\alpha - (k_z c/\omega)\sinh\alpha]}{[\cosh\alpha - (k_z c/\omega)\sinh\alpha \pm \omega_c/\hat{\gamma}_\perp\omega]} \right. \tag{16}$$
$$\left. - \frac{\hat{p}_\perp^2}{2\hat{\gamma}_\perp^2 m^2c^2} \frac{(1 - c^2k_z^2/\omega^2)}{[\cosh\alpha - (k_z c/\omega)\sinh\alpha \pm \omega_c/\hat{\gamma}_\perp\omega]^2} \right\} \ ,$$

where $\hat{\gamma}_\perp = (1 + \hat{p}_\perp^2/m^2c^2)^{\frac{1}{2}}$ is defined in Eq.(12). The limits of integration ($\pm\hat{\alpha}$) in Eq.(16) are determined from $\hat{p}_z = (\hat{\gamma}_\perp mc)\sinh\hat{\alpha}$. Because $\hat{\gamma} = \hat{\gamma}_\perp\cosh\hat{\alpha}$, where $\hat{\gamma}$ is defined in Eq.(8), the equation determining $\hat{\alpha}$ can also be expressed as

$$\hat{\beta}_z = \frac{\hat{p}_z}{\hat{\gamma}mc} = \tanh\hat{\alpha} \ . \tag{17}$$

Solving Eq.(17) for $\hat{\alpha}$ in terms of $\hat{\beta}_z$ gives

$$\hat{\alpha} = \frac{1}{2}\,\ell n\left(\frac{1 + \hat{\beta}_z}{1 - \hat{\beta}_z}\right) \ . \tag{18}$$

The integrations over α in Eq.(16) can be carried out in closed analytical

form (Appendix A). Substituting Eqs.(A.4), (A.6) and (A.7) into Eq.(16) gives the desired dispersion relation

$$0 = D_T^{\pm}(\omega,k_z) = 1 - \frac{c^2k_z^2}{\omega^2} - \frac{\omega_p^2/\hat{\gamma}}{\omega^2}\left\{G(\hat{\beta}_z) \mp \frac{\omega_c/\hat{\gamma}}{\omega(1-\hat{\beta}_z^2) \pm \omega_c/\hat{\gamma}}\, G(\xi^{\pm})\right.$$
$$\left. - \frac{\hat{\beta}_\perp^2}{2}\,\frac{(c^2k_z^2-\omega^2)}{(\omega_c/\hat{\gamma})^2 + (1-\hat{\beta}_z^2)(c^2k_z^2-\omega^2)} \right.$$
$$\left. \times \left[\frac{\omega(\omega \pm \omega_c/\hat{\gamma}) - c^2k_z^2}{(\omega \pm \omega_c/\hat{\gamma})^2 - c^2k_z^2\hat{\beta}_z^2} \mp \frac{\omega_c/\hat{\gamma}}{\omega(1-\hat{\beta}_z^2) \pm \omega_c/\hat{\gamma}}\, G(\xi^{\pm})\right]\right\} , \tag{19}$$

where $\xi^{\pm}$ is defined by

$$\xi^{\pm} = \frac{\hat{\beta}_z[(\omega_c/\hat{\gamma})^2 + (1-\hat{\beta}_z^2)(c^2k_z^2-\omega^2)]^{\frac{1}{2}}}{\omega(1-\hat{\beta}_z^2) \pm \omega_c/\hat{\gamma}} , \tag{20}$$

and $G(\xi)$ is defined by

$$G(\xi) = \frac{1}{2\xi}\ln\left(\frac{1+\xi}{1-\xi}\right) . \tag{21}$$

In Eq.(19), the various quantities are defined by $\hat{\beta}_\perp = \hat{p}_\perp/\hat{\gamma}mc$ [Eq.(8)], $\hat{\beta}_z = \hat{p}_z/\hat{\gamma}mc$ [Eq.(8)], $\hat{\gamma} = (1 + \hat{p}_\perp^2/m^2c^2 + \hat{p}_z^2/m^2c^2)^{\frac{1}{2}}$ [Eq.(8)], and $G(\hat{\beta}_z)$ is defined in Eq.(11). The fully relativistic dispersion relation (19) can be used to investigate detailed properties of the electron whistler and cyclotron maser instabilities for a wide range of effective energy anisotropy $\hat{\beta}_\perp^2/2\hat{\beta}_z^2$, normalized density ω_p^2/ω_c^2, electron energy $\hat{\gamma}mc^2$, etc.

Because $F_1(p_z)$ is an even function of p_z in Eqs.(6) and (7), it follows that the average flow velocity in the z-direction is $V_d \equiv \int d^3p(p_z/\gamma m) \times F(p_\perp^2,p_z) = 0$. For electrons with average axial velocity $V_d \equiv$ const. $\neq 0$,

the corresponding dispersion relation for a displaced waterbag distribution is readily derived from Eq.(19) by making the appropriate Lorentz transformation of ω and k_z. In particular, we view Eq.(19) as the dispersion equation relating ω and k_z in a frame of reference moving with axial velocity V_d relative to the laboratory. Then the corresponding dispersion equation relating ω' and k_z' in the laboratory frame is obtained by making the transformation

$$\omega = \gamma_d(\omega' - k_z'V_d) \ ,$$
$$k_z = \gamma_d(k_z' - \omega'V_d/c^2) \ , \tag{22}$$

in Eqs.(19) and (20). Here, γ_d is defined by $\gamma_d = (1 - V_d^2/c^2)^{-\frac{1}{2}}$, and $\omega^2 - c^2k_z^2 \to \omega'^2 - c^2k_z'^2$; $\omega \mp \omega_c/\hat{\gamma} \to \gamma_d(\omega' - k_z'V_d \mp \omega_c/\hat{\gamma}\gamma_d)$; etc.

For completeness, it is useful to simplify Eq.(19) in various limiting regimes.

C. Limiting Forms of Dispersion Relation

We consider the full dispersion relation (19) in two limiting cases: (a) zero parallel temperature ($\hat{\beta}_z = 0$), and (b) zero magnetic field ($B_0 = 0$).

Zero Parallel Temperature: For $\hat{\beta}_z = 0$, the case of maximum energy anisotropy, we obtain $G(\hat{\beta}_z) \to 1$ [Eq.(11)], $\hat{\gamma} \to \hat{\gamma}_\perp$ [Eq.(8)], and $G(\xi^\pm) \to 1$ [Eq. (21)]. For $\hat{\beta}_z \to 0$, the dispersion relation (19) reduces to[1]

$$0 = D_T^\pm(\omega,k_z) = 1 - \frac{c^2k_z^2}{\omega^2}$$
$$- \frac{\omega_p^2/\hat{\gamma}_\perp}{\omega(\omega \pm \omega_c/\hat{\gamma}_\perp)}\left[1 + \frac{\hat{\beta}_\perp^2}{2}\frac{(c^2k_z^2 - \omega^2)}{\omega(\omega \pm \omega_c/\hat{\gamma}_\perp)}\right] \ . \tag{23}$$

Zero Magnetic Field: In the case where $B_0 = 0$ and the perpendicular and parallel motions are allowed to be relativistic, we set $\omega_c = 0$ in Eq.(19), which gives the dispersion relation[15]

$$0 = D_T^{\pm}(\omega, k_z) = 1 - \frac{c^2 k_z^2}{\omega^2} - \frac{\omega_p^2/\hat{\gamma}}{\omega^2}\left[G(\hat{\beta}_z) - \frac{\hat{\beta}_\perp^2}{2(1 - \hat{\beta}_z^2)}\left(\frac{\omega^2 - c^2 k_z^2}{\omega^2 - c^2 k_z^2 \hat{\beta}_z^2} \right) \right] . \tag{24}$$

Equation (23) gives the familiar Weibel instability[14,15] in the field-free case. Of course, for $\omega_c = 0$ and $\hat{\beta}_z = 0$, Eqs.(23) and (24) are identical.

III. ELECTROMAGNETIC STABILITY PROPERTIES

In this section, we investigate the detailed stability properties predicted by the electromagnetic dispersion relation (19) for a wide range of effective energy anisotropy $\hat{\beta}_\perp^2/2\hat{\beta}_z^2$, normalized density ω_p^2/ω_c^2, and electron energy $\hat{\gamma}mc^2$. As a reference case, we first consider the case of extreme energy anisotropy where $\hat{\beta}_z = 0$. That is, the thermal speed in the z-direction is effectively zero.

A. Extreme Energy Anisotropy ($\hat{\beta}_z = 0$)

For $\hat{\beta}_z = 0$, the full dispersion relation (19) reduces to Eq.(23), which can be expressed in the equivalent form[1]

$$(\omega^2 - c^2k_z^2)\left[1 + \frac{\hat{\beta}_\perp^2}{2}\frac{\omega_p^2/\hat{\gamma}_\perp}{(\omega - \omega_c/\hat{\gamma}_\perp)^2}\right] = \frac{\omega}{(\omega - \omega_c/\hat{\gamma}_\perp)}\frac{\omega_p^2}{\hat{\gamma}_\perp} \quad . \tag{25}$$

In Eq.(25), without loss of generality, we have restricted attention to the branch with right-circular polarization [lower sign in Eq.(23)].

For $\hat{\beta}_\perp^2 = 0$ (cold-plasma limit), Eq.(25) supports only stable oscillations ($\mathrm{Im}\omega = 0$) corresponding to a fast-wave branch (the upper curve in Fig. 2), and a slow-wave branch (the lower curve in Fig. 2) which we refer to as the "whistler" mode or the "cyclotron" mode in the present analysis. In Fig. 2, $\mathrm{Re}\omega/\omega_p$ is plotted versus ck_z/ω_p for $\omega_p/\omega_c = 0.5$, 1 and 5. For $\hat{\beta}_\perp = 0$ and $\hat{\gamma}_\perp = 1$, we note from Eq.(25) and Fig. 2 that the whistler mode asymptotes at $\mathrm{Re}\omega = \omega_c$ for $c^2k_z^2/\omega_p^2 >> 1$. On the other hand, the fast-wave branch begins at $\mathrm{Re}\omega = (1/2)[\omega_c + (4\omega_p^2 + \omega_c^2)^{\frac{1}{2}}]$ for $c^2k_z^2/\omega_p^2 << 1$, and asymptotes at $\mathrm{Re}\omega = ck_z$ for $c^2k_z^2/\omega_p^2 >> 1$.

For $\hat{\beta}_\perp^2 \neq 0$, however, and moderate electron density, both the fast-wave branch and the whistler mode exhibit instability in Eq.(25). In particular, it is found (Fig. 3) that the fast-wave branch becomes unstable at long axial wavelengths (sufficiently small values of $c^2k_z^2/\omega_p^2$), whereas the whistler mode becomes unstable at short axial wavelengths (sufficiently large values of $c^2k_z^2/\omega_p^2$). The unstable fast-wave mode is referred to as the cyclotron maser instability, whereas the unstable whistler mode is referred to as the whistler instability. Typical numerical results obtained from Eq.(25) are illustrated in Fig. 3 where $Re\omega/\omega_p$ [Fig. 3(a)] and $Im\omega/\omega_p$ [Figs. 3(b) and 3(c)] are plotted versus ck_z/ω_p for $\omega_p/\omega_c = 0.5$ and $\hat{\beta}_\perp^2 = 0.2$, 0.5 and 0.9. Note in Fig. 3 that separate plots of the growth rate curves are presented for the whistler instability [Fig. 3(b)] and the cyclotron maser instability [Fig. 3(c)]. For specified values of ω_p/ω_c and $\hat{\beta}_\perp^2$, a striking feature of Fig. 3(a) is that the real frequency $Re\omega$ remains approximately constant over the range of unstable wavenumbers (k_z) for both the whistler and cyclotron maser instabilities. Moreover, for $\hat{\beta}_z = 0$, it is evident from Fig. 3(b) that the maximum growth rate of the whistler instability occurs for $c^2k_z^2/\omega_p^2 \gg 1$. Taking $c^2k_z^2 \to \infty$ in the dispersion relation (25) readily gives

$$(Im\omega)_{MAX} = \left(\frac{\hat{\beta}_\perp^2}{2\hat{\gamma}_\perp}\right)^{\frac{1}{2}} \omega_p \ ,$$

$$(Re\omega)_{MAX} = \omega_c/\hat{\gamma}_\perp \ , \qquad (26)$$

for the whistler instability at maximum growth. In units of ω_p, it follows from Eq.(26) and $\hat{\gamma}_\perp = (1 - \hat{\beta}_\perp^2)^{-\frac{1}{2}}$ that the maximum whistler growth rate assumes its absolute maximum value of $0.439\ \omega_p$ for $\hat{\beta}_\perp^2 = 2/3$ (Fig. 4).

In contrast, maximum growth of the cyclotron maser instability occurs for $k_z = 0$ [Fig. 3(c)]. Moreover, the bandwidth of the cyclotron maser instability is restricted to the wavenumber range $c^2k_z^2/\omega_p^2 \lesssim O(1)$ for the choice of parameters in Fig. 3.

For $\hat{\beta}_\perp^2 \neq 0$, and sufficiently large values of ω_p^2/ω_c^2, it is found from Eq.(25) that the cyclotron maser instability is completely stabilized, whereas the whistler mode remains unstable. This is illustrated in Fig. 5 for the case where $\omega_p^2/\omega_c^2 = 5$. Here, $Re\omega/\omega_p$ [Fig. 5(a)] and $Im\omega/\omega_p$ [Fig. 5(b)] are plotted versus ck_z/ω_p for $\hat{\beta}_\perp^2 = 0.2$, 0.5 and 0.9. The unstable mode in Fig. 5(b) corresponds to the whistler instability, whereas $Im\omega = 0$ exactly for the fast-wave branch.

The density threshold for stabilization of the cyclotron maser instability can be calculated exactly in terms of $\hat{\beta}_\perp^2$ from Eq.(25). We take $k_z = 0$ in Eq.(25), which corresponds to maximum growth rate of the cyclotron maser instability[1] when $\hat{\beta}_z = 0$. This gives

$$0 = (\omega - \omega_c/\hat{\gamma}_\perp)^3 + \frac{\omega_c}{\hat{\gamma}_\perp}(\omega - \omega_c/\hat{\gamma}_\perp)^2 + \frac{\omega_p^2}{\hat{\gamma}_\perp}\left(\frac{\hat{\beta}_\perp^2}{2} - 1\right)(\omega - \omega_c/\hat{\gamma}_\perp) + \frac{\omega_c}{\hat{\gamma}_\perp}\frac{\omega_p^2}{\hat{\gamma}_\perp}\frac{\hat{\beta}_\perp^2}{2} . \tag{27}$$

Equation (27) determines the real frequency $Re\omega$ and growth rate $Im\omega$ of the cyclotron maser instability at maximum growth ($k_z = 0$). Some straightforward algebra shows that the necessary and sufficient condition for stability ($Im\omega = 0$) is given by

$$\frac{\omega_p^2}{\omega_c^2} \geq \frac{\omega_p^2}{\omega_c^2}\bigg|_{cr} \equiv \frac{(1 - \hat{\beta}_\perp^2)^{\frac{1}{2}}}{(2 - \hat{\beta}_\perp^2)^3}\left[2\hat{\beta}_\perp^4 + 10\hat{\beta}_\perp^2 - 1 + (64\hat{\beta}_\perp^6 + 48\hat{\beta}_\perp^4 + 12\hat{\beta}_\perp^2 + 1)^{\frac{1}{2}}\right] . \tag{28}$$

That is, whenever ω_p^2/ω_c^2 exceeds the critical value in Eq.(28), the cyclotron maser instability is completely stabilized. This is illustrated in Fig. 6, which shows the regions of $(\hat{\beta}_\perp^2, \omega_p^2/\omega_c^2)$ parameter space corresponding to stability and instability.

Equation (27) can also be used to determine the real frequency and growth rate of the cyclotron maser instability at maximum growth as functions of ω_p/ω_c and $\hat{\beta}_\perp^2$. Typical results are illustrated in Figs. 7 and 8. In Fig. 7, plots of $Re\omega/\omega_p$ [Fig. 7(a)] and $Im\omega/\omega_p$ [Fig. 7(b)] versus ω_p/ω_c obtained from Eq.(27) are presented for $\hat{\beta}_\perp^2 = 0.2$, 0.5 and 0.9. (Note that $Re\omega/\omega_p$ is plotted only for the unstable ranges of ω_p/ω_c.) Consistent with Eq.(28) and Fig. 6, it is clear from Fig. 7(b) that the instability bandwidth (in ω_p/ω_c - space) decreases as $\hat{\beta}_\perp^2$ is reduced. Similarly, Fig. 8 shows plots of $Re\omega/\omega_p$ [Fig. 8(a)] and $Im\omega/\omega_p$ [Fig. 8(b)] versus $\hat{\beta}_\perp^2$ obtained from Eq.(27) for $\omega_p/\omega_c = 0.5$, 1 and 2. Evidently, consistent with Eq. (28) and Fig. 6, the instability bandwidth (in $\hat{\beta}_\perp^2$ - space) and maximum growth rate decrease as ω_p/ω_c is increased.

B. Arbitrary Energy Anisotropy

Electromagnetic stability properties were examined in Sec. III.A for the case of extreme energy anisotropy ($\hat{\beta}_z = 0$). In this section, we make use of the electromagnetic dispersion relation (19) to investigate detailed stability properties for finite values of the anisotropy factor $\hat{\beta}_\perp^2/2\hat{\beta}_z^2$.

In particular, Eq.(19) is solved numerically for the real oscillation frequency $\mathrm{Re}\omega$ and growth rate $\mathrm{Im}\omega$ for both the cyclotron maser and whistler branches over a wide range of system parameters ω_p^2/ω_c^2 and $\hat{\beta}_\perp^2/2\hat{\beta}_z^2$.

Typical results are illustrated in Fig. 9 for the choice of system parameters $\omega_p^2/\omega_c^2 = 0.25$ and $\hat{\beta}_\perp^2 = 0.5$. In Fig. 9(a), the normalized real oscillation frequency $\mathrm{Re}\omega/\omega_p$ is plotted versus ck_z/ω_p for the case $\hat{\beta}_\perp^2/2\hat{\beta}_z^2 = 11$. The dashed portions of the dispersion curves in Fig. 9(a) correspond to the unstable range of wavenumbers for the cyclotron maser and whistler instabilities. Further detail is presented in Figs. 9(b) - 9(e). In particular, shown in Figs. 9(b) and 9(c) for the electron whistler branch are plots of $\mathrm{Re}\omega/\omega_p$ [Fig. 9(b)] and $\mathrm{Im}\omega/\omega_p$ [Fig. 9(c)] versus ck_z/ω_p obtained from Eq.(19) for anisotropy factors ranging from $\hat{\beta}_\perp^2/2\hat{\beta}_z^2 = \infty$ to $\hat{\beta}_\perp^2/2\hat{\beta}_z^2 = 1$. We note from Fig. 9(c) that the maximum growth rate and the range of unstable k_z values decrease with decreasing values of $\hat{\beta}_\perp^2/2\hat{\beta}_z^2$. Moreover, there is a corresponding decrease in $\mathrm{Re}\omega/\omega_p$ as $\hat{\beta}_\perp^2/2\hat{\beta}_z^2$ is reduced [Fig. 9(b)]. For $\hat{\beta}_\perp^2 = 0.5$ and $\omega_p^2/\omega_c^2 = 0.25$, it is found from Eq.(19) that the whistler instability is completely stabilized when the anisotropy factor is reduced to $\hat{\beta}_\perp^2/2\hat{\beta}_z^2 = 0.506$. Finally, shown in Figs. 9(d) and 9(e) for the cyclotron maser branch are plots of $\mathrm{Re}\omega/\omega_p$ [Fig 9(d)] and $\mathrm{Im}\omega/\omega_p$ [Fig. 9(e)] versus ck_z/ω_p obtained from Eq.(19) for anisotropy factors ranging from $\hat{\beta}_\perp^2/2\hat{\beta}_z^2 = \infty$ to $\hat{\beta}_\perp^2/2\hat{\beta}_z^2 = 0.51$. We note from Fig. 9(d) that $\mathrm{Re}\omega/\omega_p$ decreases as the anisotropy factor $\hat{\beta}_\perp^2/2\hat{\beta}_z^2$ is reduced. Moreover, the normalized growth rate $\mathrm{Im}\omega/\omega_p$ decreases as $\hat{\beta}_\perp^2/2\hat{\beta}_z^2$ is reduced [Fig. 9(e)]. Indeed, for $\hat{\beta}_\perp^2 = 0.5$ and $\omega_p^2/\omega_c^2 = 0.25$, it is found from Eq.(19) that complete stabilization of the cyclotron maser instability requires reduction of the anisotropy factor to $\hat{\beta}_\perp^2/2\hat{\beta}_z^2 = 0.50$, corresponding to $\hat{\gamma} \to \infty$. For general values of $\hat{\beta}_\perp^2/2\hat{\beta}_z^2$, we also note

from Eq.9(e) that maximum growth of the cyclotron maser instability always occurs for $k_z = 0$. [Compare with Fig. 3(c) for the special case where $\hat{\beta}_z = 0$.]

Similar stability plots obtained from Eq.(19) are presented in Fig. 10 for the case where $\hat{\beta}_\perp^2 = 0.5$ and the value of ω_p^2/ω_c^2 is increased to $\omega_p^2/\omega_c^2 = 5$. For this choice of system parameters, ω_p^2/ω_c^2 is sufficiently large that the cyclotron maser instability is absent ($Im\omega = 0$) for all values of the anisotropy factor $\hat{\beta}_\perp^2/2\hat{\beta}_z^2$. For the electron whistler branch, $Re\omega/\omega_p$ and $Im\omega/\omega_p$ are plotted versus ck_z/ω_p in Figs. 10(a) and 10(b), respectively, for values of the anisotropy factor ranging from $\hat{\beta}_\perp^2/2\hat{\beta}_z^2 = \infty$ to $\hat{\beta}_\perp^2/2\hat{\beta}_z^2 = 0.69$. The qualitative features of the stability behavior in Fig. 10 are similar to Figs. 9(b) and 9(c), i.e., the real oscillation frequency, the growth rate, and the instability bandwidth (in k_z-space) all decrease as the anisotropy factor $\hat{\beta}_\perp^2/2\hat{\beta}_z^2$ is reduced. Moreover, we note that the normalized growth rates $Im\omega/\omega_p$ in Fig. 10(b) (obtained for $\omega_p^2/\omega_c^2 = 5$) are comparable in magnitude to those in Fig. 9(c) (obtained for $\omega_p^2/\omega_c^2 = 0.25$). On the other hand, comparing Figs. 9(b) and 10(a), the real oscillation frequency (measured in units of ω_p) is reduced substantially as ω_p^2/ω_c^2 is increased. For the choice of system parameters in Fig. 10, it is found from Eq.(19) that the whistler instability is completely stabilized when the anisotropy factor is reduced to $\hat{\beta}_\perp^2/2\hat{\beta}_z^2 = 0.51$.

For the cyclotron maser branch, Fig. 11 illustrates the scaling of stability properties with ω_p^2/ω_c^2. In particular, shown in Fig. 11 are plots of $Re\omega/\omega_p$ [Fig. 11(a)] and $Im\omega/\omega_p$ [Fig. 11(b)] versus ck_z/ω_p obtained from Eq.(19) for $\hat{\beta}_\perp^2 = 0.5$, $\hat{\beta}_\perp^2/2\hat{\beta}_z^2 = 1.56$ (which corresponds to $\hat{\beta}_z^2 = 0.160$ when $\hat{\beta}_\perp^2 = 0.5$), and values of normalized density ranging from $\omega_p^2/\omega_c^2 = 0.25$ to $\omega_p^2/\omega_c^2 = 1$. It is evident from Fig. 11 that the real oscillation frequency, growth rate, and bandwidth (in k_z-space) all decrease as ω_p^2/ω_c^2 is increased.

Indeed, for the choice of system parameters in Fig. 11, the cyclotron maser instability is completely stabilized when the normalized density is increased to $\omega_p^2/\omega_c^2 = 2.3$.

Similarly, Fig. 12 shows the scaling of stability properties with ω_p^2/ω_c^2 calculated from Eq.(19) for the whistler branch. In particular, $Re\omega/\omega_p$ and $Im\omega/\omega_p$ are plotted versus ck_z/ω_p in Figs. 12(a) and 12(b), respectively, for the choice of system parameters $\hat{\beta}_\perp^2 = 0.5$, $\hat{\beta}_\perp^2/2\hat{\beta}_z^2 = 11$ (which corresponds to $\hat{\beta}_z^2 = 0.0227$ when $\hat{\beta}_\perp^2 = 0.5$), and values of normalized density ranging from $\omega_p^2/\omega_c^2 = 0.25$ to $\omega_p^2/\omega_c^2 = 25$. We note that $Re\omega/\omega_p$ decreases as ω_p^2/ω_c^2 is increased [Fig. 12(a)], and there is a concomitant downshift in k_z of the growth rate curves [Fig. 12(b)]. Indeed, in the limit of zero magnetic field ($\omega_p^2/\omega_c^2 \to \infty$), the whistler instability in Fig. 12 evolves continuously into the classical Weibel instability[13-15] with $Re\omega = 0$, and nonzero growth rate ($Im\omega \neq 0$) over a finite bandwidth in k_z-space.

The dispersion relation (19) can also be used to determine the stability boundaries separating the regions of parameter space corresponding to stability ($Im\omega = 0$) and instability ($Im\omega > 0$). Shown in Fig. 13 are the regions of $(\hat{\beta}_\perp^2, \omega_p^2/\omega_c^2)$ parameter space corresponding to stability and instability for the cyclotron maser mode. The stability boundaries in Fig. 13 are calculated from Eq.(19) for several values of $\hat{\beta}_z$. For specified $\hat{\beta}_z$, the region above the curve in Fig. 13 corresponds to stability. As in the case $\hat{\beta}_z = 0$ (Fig. 6), for specified value of $\hat{\beta}_\perp^2$, it is evident from Fig. 13 that there exists a critical value of ω_p^2/ω_c^2 above which the cyclotron maser instability is completely stabilized. Note also from Fig. 13 that the unstable region of $(\hat{\beta}_\perp^2, \omega_p^2/\omega_c^2)$ parameter space continues to decrease in area as $\hat{\beta}_z$ is increased and the anisotropy factor $\hat{\beta}_\perp^2/2\hat{\beta}_z^2$ is reduced.

Finally, shown in Fig. 14 are the regions of $(2\hat{\beta}_z^2, \hat{\beta}_\perp^2)$ parameter space corresponding to stability and instability for the whistler mode. The stability boundaries in Fig. 14 are calculated from Eq.(19) for several values of ω_p^2/ω_c^2. For specified ω_p^2/ω_c^2, the region above the curve starting at the origin in Fig. 14 corresponds to instability ($Im\omega > 0$). That is, the anisotropy factor $\hat{\beta}_\perp^2/2\hat{\beta}_z^2$ is large enough in this region to give instability. As ω_p^2/ω_c^2 is decreased from $\omega_p^2/\omega_c^2 = \infty$ (corresponding to $B_0 = 0$), it is evident from Fig. 14 that smaller values of the anisotropy factor $\hat{\beta}_\perp^2/2\hat{\beta}_z^2$ are required to stabilize the whistler instability.

IV. DISPERSION RELATION FOR THERMAL EQUILIBRIUM DISTRIBUTION IN PARALLEL MOMENTUM

For completeness, in this section we simplify the dispersion relation (4) for the case where the parallel momentum distribution $F_1(p_z)$ corresponds to the thermal equilibrium distribution

$$F_1(p_z) = \frac{\exp(-\gamma mc^2/T_z)}{2\hat{\gamma}_\perp mcK_1(\hat{\gamma}_\perp mc^2/T_z)} \ . \tag{29}$$

Here, T_z = const. is the parallel temperature, $\gamma = (1 + \hat{p}_\perp^2/m^2c^2 + p_z^2/m^2c^2)^{\frac{1}{2}}$ is defined in Eq.(5), $\hat{\gamma}_\perp = (1 + \hat{p}_\perp^2/m^2c^2)^{\frac{1}{2}}$ is defined in Eq.(12), and $K_n(x)$ is the modified Bessel function of the second kind of order n. Substituting Eq.(29) into Eq.(4) gives the dispersion relation

$$0 = D_T^{\pm}(k_z,\omega) = 1 - \frac{c^2k_z^2}{\omega^2} - \frac{(\omega_p^2/\omega^2)}{2\hat{\gamma}_\perp mcK_1(\hat{\gamma}_\perp mc^2/T_z)} \int_{-\infty}^{\infty} \frac{dp_z}{\gamma}$$

$$\times \exp(-\gamma mc^2/T_z) \left\{ \frac{\gamma\omega - k_zp_z/m}{\gamma\omega - k_zp_z/m \pm \omega_c} - \frac{\hat{p}_\perp^2}{2m^2c^2} \frac{(\omega^2 - c^2k_z^2)}{(\gamma\omega - k_zp_z/m \pm \omega_c)^2} \right\} , \tag{30}$$

where $\mathrm{Im}\omega > 0$ is assumed. We express Eq.(30) in an alternate form by making use of the identities (valid for $\mathrm{Im}\omega > 0$)

$$\int_0^{\infty} d\tau \exp[i(\gamma\omega - k_zp_z/m \pm \omega_c)\tau] = \frac{i}{\gamma\omega - k_zp_z/m \pm \omega_c} \ ,$$

$$\int_0^{\infty} d\tau\tau \exp[i(\gamma\omega - k_zp_z/m \pm \omega_c)\tau] = -\frac{1}{(\gamma\omega - k_zp_z/m \pm \omega_c)^2} \ . \tag{31}$$

We further introduce the transformation $p_z = (\hat{\gamma}_\perp mc)\sinh\alpha$ and $\gamma = \hat{\gamma}_\perp \cosh\alpha$ defined in Eqs.(14) and (15). Equation (30) can then be expressed in the equivalent form

$$0 = D_T^{\pm}(k_z,\omega) = 1 - \frac{c^2k_z^2}{\omega^2} + \frac{i(\omega_p^2/\omega^2)}{2\hat{\gamma}_\perp mcK_1(\hat{\gamma}_\perp mc^2/T_z)}$$

$$\times \int_0^\infty d\tau \exp[\pm i(\omega_c/\hat{\gamma}_\perp)\tau] \int_{-\infty}^{\infty} d\alpha \exp[-(\hat{\gamma}_\perp mc^2/T_z - i\omega\tau)\cosh\alpha - ick_z\tau\sinh\alpha] \qquad (32)$$

$$\times \left\{ \cosh\alpha - \frac{ck_z}{\omega}\sinh\alpha + i\omega\tau\left(1 - \frac{c^2k_z^2}{\omega^2}\right)\frac{\hat{p}_\perp^2}{2\hat{\gamma}_\perp^2 m^2c^2} \right\} ,$$

where use has been made of Eqs.(14), (15) and (31). The integration over α in Eq.(32) can be carried out exactly by making use of the integral transform

$$\frac{1}{\pi} K_0[(a^2 + b^2)^{\frac{1}{2}}] = \frac{1}{2\pi}\int_{-\infty}^{\infty} d\alpha \exp(-ib\sinh\alpha - a\cosh\alpha) . \qquad (33)$$

We introduce the variable ζ defined by

$$\zeta^2 = \left(\frac{\hat{\gamma}_\perp mc^2}{T_z} - i\omega\tau\right)^2 + c^2k_z^2\tau^2 . \qquad (34)$$

Then, from Eqs.(33) and (34), the dispersion relation (32) can be expressed as

$$0 = D_T^{\pm}(k_z,\omega) = 1 - \frac{\omega_p^2/\hat{\gamma}_\perp}{\omega^2}\left\{ \frac{K_0(\hat{\gamma}_\perp mc^2/T_z)}{K_1(\hat{\gamma}_\perp mc^2/T_z)} \right.$$

$$+ \frac{i}{K_1(\hat{\gamma}_\perp mc^2/T_z)}\int_0^\infty d\tau K_0(\zeta)\exp[\pm i(\omega_c/\hat{\gamma}_\perp)\tau] \qquad (35)$$

$$\left. \times \left[\pm\frac{\omega_c}{\hat{\gamma}_\perp} - i\tau(\omega^2 - c^2k_z^2)\frac{\hat{p}_\perp^2}{2\hat{\gamma}_\perp^2 m^2c^2} \right] \right\}$$

for $\mathrm{Im}\omega > 0$. Although the τ-integration in Eq.(35) cannot be carried out in closed form, this form of the dispersion relation is particularly useful for numerical solutions and for analytical approximations in various limiting regimes. A detailed analysis of Eq.(35) will be the subject of a future investigation.

As a simple limiting case, we consider Eq.(35) for $B_0 = 0$, which corresponds to the Weibel instability in an unmagnetized plasma. Some straightforward algebra that makes use of Eqs.(3) and (29) shows that T_z can be identified with the parallel temperature $\int d^3p(p_z^2/\gamma m)F(p_\perp^2,p_z)$, and that the effective perpendicular temperature $T_\perp = \int d^3p(p_\perp^2/2\gamma m)F(p_\perp^2,p_z)$ is given by

$$T_\perp = \frac{1}{2}\,\hat{\gamma} mc^2 \left(\frac{\hat{p}_\perp}{\hat{\gamma}_\perp mc}\right)^2 \frac{K_0(\hat{\gamma}_\perp mc^2/T_z)}{K_1(\hat{\gamma}_\perp mc^2/T_z)} \,. \tag{36}$$

Setting $\omega_c = 0$ in Eq.(35) and making use of Eq.(36) give the dispersion relation for an unmagnetized plasma, i.e.,

$$0 = D_T(k_z,\omega) = 1 - \frac{c^2k_z^2}{\omega^2} - \frac{(\omega_p^2/\hat{\gamma}_\perp)}{\omega^2}\left\{\frac{K_0(\hat{\gamma}_\perp mc^2/T_z)}{K_1(\hat{\gamma}_\perp mc^2/T_z)} + \frac{T_\perp}{\hat{\gamma}_\perp mc^2}\,\frac{(\omega^2 - c^2k_z^2)}{K_0(\hat{\gamma}_\perp mc^2/T_z)}\int_0^\infty d\tau\tau K_0(\zeta)\right\} \,. \tag{37}$$

The τ-integral in Eq.(37) must generally be evaluated numerically, or in the context of asymptotic expansions for large or small values of $|\zeta|$. Unlike Eq.(19), the dispersion relation (37) generally incorporates the effects of collisionless dissipation (Landau damping) by the p_z distribution in Eq.(29). For the slow-wave branch, it can be shown from Eq.(37) that the necessary and sufficient condition for instability is given by

$$\frac{T_\perp}{T_z} > \left[\frac{K_0(\hat{\gamma}_\perp mc^2/T_z)}{K_1(\hat{\gamma}_\perp mc^2/T_z)}\right]^2 , \tag{38}$$

where $T_\perp$ is defined in Eq.(36). Moreover, when Eq.(38) is satisfied, it is found that $\mathrm{Re}\omega = 0$ (for the slow-wave branch) over the range of unstable wavenumbers specified by

$$0 < k_z^2 < k_0^2 \equiv \frac{\omega_p^2}{\hat{\gamma}_\perp c^2}\left[\frac{T_\perp}{T_z}\frac{K_1(\hat{\gamma}_\perp mc^2/T_z)}{K_0(\hat{\gamma}_\perp mc^2/T_z)} - \frac{K_0(\hat{\gamma}_\perp mc^2/T_z)}{K_1(\hat{\gamma}_\perp mc^2/T_z)}\right] . \tag{39}$$

Note from Eq.(39) that the marginal stability point k_0^2 (where $\mathrm{Im}\omega = 0 = \mathrm{Re}\omega$) can be calculated in closed analytical form. This follows from the identity

$$\lim_{\mathrm{Im}\omega \to 0_+}\left[c^2k_z^2\int_0^\infty d\tau\tau K_0(\zeta)\right]_{\mathrm{Re}\omega = 0} = \frac{\hat{\gamma}_\perp mc^2}{T_z}K_1(\hat{\gamma}_\perp mc^2/T_z) . \tag{40}$$

Finally, shown in Fig. 15 is a plot of the stability boundary in the parameter space $(T_z/\hat{\gamma}_\perp mc^2,\ T_\perp/\hat{\gamma}_\perp mc^2)$ calculated numerically from Eq.(38). The region above the curve in Fig. 15 corresponds to instability, which requires sufficiently large thermal anisotropy $T_\perp/T_z$.

V. CONCLUSIONS

Detailed properties of the cyclotron maser and whistler instabilities in a relativistic magnetized plasma have been investigated for the particular choice of anisotropic, "waterbag" distribution function $F(p_\perp^2, p_z)$ in Eq.(7), which permits an exact analytical reduction of the dispersion relation (2) for arbitrary energy anisotropy (Sec. II). The resulting dispersion relation in Eq.(19) was solved numerically, and detailed properties of the cyclotron maser and whistler instabilities were determined over a wide range of effective energy anisotropy $\hat{\beta}_\perp^2/2\hat{\beta}_z^2$ and normalized density ω_p^2/ω_c^2 (Sec. III). Not only does the choice of waterbag distribution in Eq.(7) readily permit the calculation of detailed stability properties over a wide range of system parameters, the corresponding dispersion relation (19) can be used to determine universal stability boundaries for the cyclotron maser and whistler instabilities. For example, Figs. 6 and 13 show the stability boundaries for the cyclotron maser instability in $(\hat{\beta}_\perp^2, \omega_p^2/\omega_c^2)$ parameter space for several values of $\hat{\beta}_z$. Similarly, the stability boundaries for the whistler instability in $(2\hat{\beta}_z^2, \hat{\beta}_\perp^2)$ parameter space are illustrated in Fig. 14 for several values of ω_p^2/ω_c^2. Finally, the electromagnetic dispersion relation (35) was derived for the case where the parallel momentum distribution $F_1(p_z)$ corresponds to the thermal equilibrium distribution in Eq.(29) (Sec. IV). A detailed analysis of Eq.(35) will be the subject of a future investigation.

ACKNOWLEDGMENTS

This research was supported in part by the Department of Energy and in part by the Office of Naval Research.

VI. REFERENCES

1. K.R. Chu and J.L. Hirschfield, Phys. Fluids 21, 461 (1978).
2. H.S. Uhm, R.C. Davidson and K.R. Chu, Phys. Fluids 21, 1866 (1978).
3. C.S. Wu and L.C. Lee, Astrophys. J. 230, 621 (1979).
4. L.C. Lee and C.S. Wu, Phys. Fluids 23, 1348 (1980).
5. Y.Y. Lau and K.R. Chu, Phys. Rev. Lett. 50, 243 (1983).
6. K.T. Tsang, Phys. Fluids 27, 1659 (1984).
7. P.L. Pritchett, Phys. Fluids 27, 2393 (1984).
8. H.K. Wong, C.S. Wu and J.D. Gaffey, Jr., Phys. Fluids 28, 2751 (1985).
9. H.S. Uhm and R.C. Davidson, Phys. Fluids 29, 2713 (1986).
10. R.N. Sudan, Phys. Fluids 6, 57 (1963).
11. C.F. Kennel and H.E. Petschek, J. Geophys. Res. 72, 3303 (1967).
12. N.T. Gladd, Phys. Fluids 26, 974 (1983), and references therein.
13. R.C. Davidson, Handbook of Plasma Physics, Volume 1 (A.A. Galeev and R.N. Sudan, eds., North-Holland Publishing Co., New York, 1983) pp. 521-585; cf., pp. 552-573, and references therein.
14. E.S. Weibel, Phys. Rev. Lett. 2, 83 (1959).
15. P.H. Yoon and R.C. Davidson, Phys. Rev. A34, in press (1986).

APPENDIX A

EVALUATION OF AXIAL MOMENTUM INTEGRALS

We evaluate here the integrals over α required to simplify the dispersion relation (16). In this regard, it is useful to introduce the definite integrals defined by

$$I_1 \equiv \int_{-\hat{\alpha}}^{\hat{\alpha}} \frac{d\alpha}{(a + b\cosh\alpha + d\sinh\alpha)} , \tag{A.1}$$

$$I_2 \equiv \int_{-\hat{\alpha}}^{\hat{\alpha}} d\alpha \frac{(b\cosh\alpha + d\sinh\alpha)}{(a + b\cosh\alpha + d\sinh\alpha)} , \tag{A.2}$$

$$I_3 \equiv \int_{-\hat{\alpha}}^{\hat{\alpha}} \frac{d\alpha}{(a + b\cosh\alpha + d\sinh\alpha)^2} , \tag{A.3}$$

where $\sinh\hat{\alpha} = \hat{p}_z/\hat{\gamma}_\perp mc$, $a = \pm\omega_c/\hat{\gamma}_\perp\omega$, $b = 1$, and $d = -ck_z/\omega$. Some straightforward algebra shows that

$$I_1 = \frac{1}{(a^2 + d^2 - b^2)^{\frac{1}{2}}} \ln\left[\frac{(a - b)\tanh(\alpha/2) - d + (a^2 + d^2 - b^2)^{\frac{1}{2}}}{(a - b)\tanh(\alpha/2) - d - (a^2 + d^2 - b^2)^{\frac{1}{2}}}\right]\Bigg|_{-\hat{\alpha}}^{\hat{\alpha}}$$

$$= \frac{\omega(1 - \hat{\beta}_z^2)^{\frac{1}{2}}}{[(\omega_c/\hat{\gamma})^2 + (1 - \hat{\beta}_z^2)(c^2k_z^2 - \omega^2)]^{\frac{1}{2}}} \tag{A.4}$$

$$\times \ln\left[\frac{\omega(1 - \hat{\beta}_z^2) \pm \omega_c/\hat{\gamma} + \hat{\beta}_z[(\omega_c/\hat{\gamma})^2 + (1 - \hat{\beta}_z^2)(c^2k_z^2 - \omega^2)]^{\frac{1}{2}}}{\omega(1 - \hat{\beta}_z^2) \pm \omega_c/\hat{\gamma} - \hat{\beta}_z[(\omega_c/\hat{\gamma})^2 + (1 - \hat{\beta}_z^2)(c^2k_z^2 - \omega^2)]^{\frac{1}{2}}}\right] .$$

Moreover, from Eqs.(A.1) and (A.2), I_2 can be expressed in terms of I_1 by

$$I_2 = 2\hat{\alpha} - aI_1 \ . \tag{A.5}$$

Making use of $\sinh\hat{\alpha} = \hat{p}_z/\hat{\gamma}_\perp mc = (\hat{\gamma}/\hat{\gamma}_\perp)\hat{\beta}_z = (\cosh\hat{\alpha})\hat{\beta}_z$ gives $2\hat{\alpha} = \ln[(1 + \hat{\beta}_z)/(1 - \hat{\beta}_z)]$. For $a = \pm\omega_c/\hat{\gamma}_\perp\omega$, Eq.(A.5) then becomes

$$I_2 = \ln\left(\frac{1 + \hat{\beta}_z}{1 - \hat{\beta}_z}\right) \mp \frac{\omega_c/\hat{\gamma}}{\omega(1 - \hat{\beta}_z^2)^{\frac{1}{2}}} I_1 \ , \tag{A.6}$$

where I_1 is defined in Eq.(A.4). Finally, making use of Eq.(A.3), it can be shown that I_3 can be expressed as

$$I_3 = -\frac{(1 - \hat{\beta}_z^2)}{2\hat{\beta}_z} \frac{\omega^2}{[\omega_c^2/\hat{\gamma}^2 + (1 - \hat{\beta}_z^2)(c^2k_z^2 - \omega^2)]} \left[\frac{\omega(\omega \pm \omega_c/\hat{\gamma}) - c^2k_z^2}{(\omega \pm \omega_c/\hat{\gamma})^2 - c^2k_z^2\hat{\beta}_z^2}\right] \tag{A.7}$$

$$\pm \frac{\omega(\omega_c/\hat{\gamma})(1 - \hat{\beta}_z^2)^{\frac{1}{2}}}{\omega_c^2/\hat{\gamma}^2 + (1 - \hat{\beta}_z^2)(c^2k_z^2 - \omega^2)} I_1 \ ,$$

where I_1 is defined in Eq.(A.4), and $\hat{\gamma}$ is defined by $\hat{\gamma} = (1 + \hat{p}_\perp^2/m^2c^2 + \hat{p}_z^2/m^2c^2)^{\frac{1}{2}}$.

Substituting the expressions for I_1, I_2 and I_3 in Eqs. (A.4), (A.6) and (A.7) into Eq.(16) gives the desired dispersion relation in Eq.(19). From the expression for $G(\xi)$ in Eq.(21), we note that the following expansions for $G(\xi)$ pertain

$$G(\xi) = \begin{cases} 1 + \dfrac{\xi^2}{3} + \dfrac{\xi^4}{5} + \cdots + \dfrac{\xi^{2n}}{(2n+1)} + \cdots \ , & |\xi| < 1 \ , \\ \dfrac{1}{\xi^2} + \dfrac{1}{3\xi^4} + \dfrac{1}{5\xi^6} + \cdots + \dfrac{1}{(2n+1)\xi^{2n+2}} + \cdots + i\dfrac{\pi}{2\xi} \ , & |\xi| > 1, \end{cases} \tag{A.8}$$

in the regions $|\xi| < 1$ and $|\xi| > 1$.

FIGURE CAPTIONS

Fig. 1. Plot of $G(\hat{\beta}_z)$ versus $\hat{\beta}_z$ [Eq.(11)].

Fig. 2. Plots of $Re\omega/\omega_p$ versus ck_z/ω_p obtained from Eq.(25) for $\hat{\beta}_z = 0 = \hat{\beta}_\perp$ and several values of ω_p/ω_c.

Fig. 3. Plots versus ck_z/ω_p of (a) $Re\omega/\omega_p$, (b) $Im\omega/\omega_p$ (whistler instability), and (c) $Im\omega/\omega_p$ (cyclotron maser instability) obtained from Eq.(25) for $\hat{\beta}_z = 0$, $\omega_p/\omega_c = 0.5$, and several values of $\hat{\beta}_\perp^2$.

Fig. 4. Plot of normalized maximum growth rate $(Im\omega)_{MAX}/\omega_p$ versus $\hat{\beta}_\perp$ for the electron whistler branch obtained from Eq.(26) for $\hat{\beta}_z = 0$ and $k_z = \infty$. The absolute maximum growth rate is $0.439\ \omega_p$, which occurs for $\hat{\beta}_\perp^2 = 2/3$.

Fig. 5. Plots versus ck_z/ω_p of (a) $Re\omega/\omega_p$, and (b) $Im\omega/\omega_p$ (whistler instability) obtained from Eq.(25) for $\hat{\beta}_z = 0$, $\omega_p^2/\omega_c^2 = 5$, and several values of $\hat{\beta}_\perp^2$. The cyclotron maser instability is absent ($Im\omega = 0$) for $\omega_p^2/\omega_c^2 = 5$ and $\hat{\beta}_z = 0$.

Fig. 6. Regions of $(\hat{\beta}_\perp^2, \omega_p^2/\omega_c^2)$ parameter space corresponding to stability ($Im\omega = 0$) and instability ($Im\omega > 0$) for the cyclotron maser mode [Eqs.(27) and (28)]. For $\hat{\beta}_z = 0$ and specified $\hat{\beta}_\perp^2 \neq 0$, the cyclotron maser instability is completely absent for sufficiently large values of ω_p^2/ω_c^2.

Fig. 7. Plots of (a) $Re\omega/\omega_p$, and (b) $Im\omega/\omega_p$ versus ω_p/ω_c obtained from Eq.(27) for the cyclotron maser mode at maximum growth ($k_z = 0$ and $\hat{\beta}_z = 0$) for several values of $\hat{\beta}_\perp^2$. $Re\omega/\omega_p$ is plotted only over the unstable range of ω_p/ω_c in Fig. 7(a).

Fig. 8. Plots of (a) $Re\omega/\omega_p$, and (b) $Im\omega/\omega_p$ versus $\hat{\beta}_\perp^2$ obtained from Eq.(27) for the cyclotron maser mode at maximum growth ($k_z = 0$ and $\hat{\beta}_z = 0$) for several values of ω_p/ω_c. $Re\omega/\omega_p$ is plotted only over the unstable range of $\hat{\beta}_\perp^2$ in Fig. 8(a).

Fig. 9. Electromagnetic stability properties calculated from Eq.(19) for $\hat{\beta}_\perp^2 = 0.5$ and $\omega_p^2/\omega_c^2 = 0.25$. Plots of (a) $Re\omega/\omega_p$ versus ck_z/ω_p for $\hat{\beta}_\perp^2/2\hat{\beta}_z^2 = 11$. Plots of (b) $Re\omega/\omega_p$, and (c) $Im\omega/\omega_p$ versus ck_z/ω_p for the whistler branch for several values of $\hat{\beta}_\perp^2/2\hat{\beta}_z^2$. Plots of (d) $Re\omega/\omega_p$, and (e) $Im\omega/\omega_p$ versus ck_z/ω_p for the cyclotron maser branch for several values of $\hat{\beta}_\perp^2/2\hat{\beta}_z^2$.

Fig. 10. Whistler stability properties calculated from Eq.(19) for $\hat{\beta}_\perp^2 = 0.5$ and $\omega_p^2/\omega_c^2 = 5$. Plots of (a) $Re\omega/\omega_p$, and (b) $Im\omega/\omega_p$ versus ck_z/ω_p for several values of $\hat{\beta}_\perp^2/2\hat{\beta}_z^2$. (The cyclotron maser instability is absent for the choice of system parameters in Fig. 10.)

Fig. 11. Cyclotron maser stability properties calculated from Eq.(19) for $\hat{\beta}_\perp^2 = 0.5$ and $\hat{\beta}_\perp^2/2\hat{\beta}_z^2 = 1.56$. Plots of (a) $Re\omega/\omega_p$, and (b) $Im\omega/\omega_p$ versus ck_z/ω_p for several values of ω_p^2/ω_c^2.

Fig. 12. Whistler stability properties calculated from Eq.(19) for $\hat{\beta}_\perp^2 = 0.5$ and $\hat{\beta}_\perp^2/2\hat{\beta}_z^2 = 11$. Plots of (a) $Re\omega/\omega_p$, and (b) $Im\omega/\omega_p$ versus ck_z/ω_p for several values of ω_p^2/ω_c^2.

Fig. 13. Regions of $(\hat{\beta}_\perp^2, \omega_p^2/\omega_c^2)$ parameter space corresponding to stability ($Im\omega = 0$) and instability ($Im\omega > 0$) for the cyclotron maser mode. The stability boundaries are calculated from Eq.(19) for several values of $\hat{\beta}_z$ (see also Fig. 6).

Fig. 14. Regions of $(2\hat{\beta}_z^2, \hat{\beta}_\perp^2)$ parameter space corresponding to stability ($Im\omega = 0$) and instability ($Im\omega > 0$) for the whistler mode. The stability boundaries are calculated from Eq.(19) for several values of ω_p^2/ω_c^2.

Fig. 15. Regions of $(T_z/\hat{\gamma}_\perp mc^2, T_\perp/\hat{\gamma}_\perp mc^2)$ parameter space corresponding to stability ($Im\omega = 0$) and instability ($Im\omega > 0$) for the slow-wave (Weibel) mode. The stability boundary is calculated from Eqs.(37) and (38) ($B_0 = 0$).

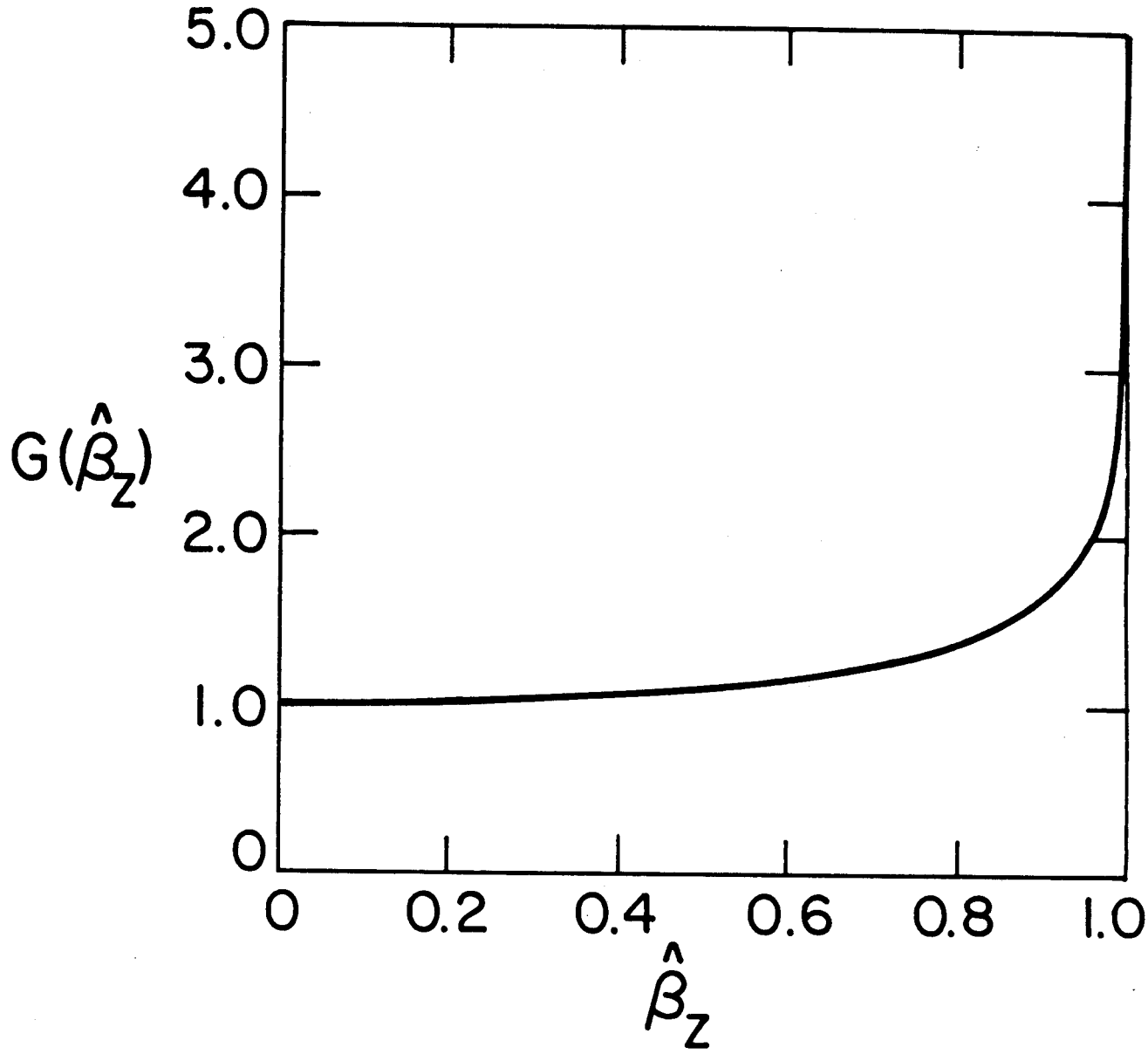

Fig. 1

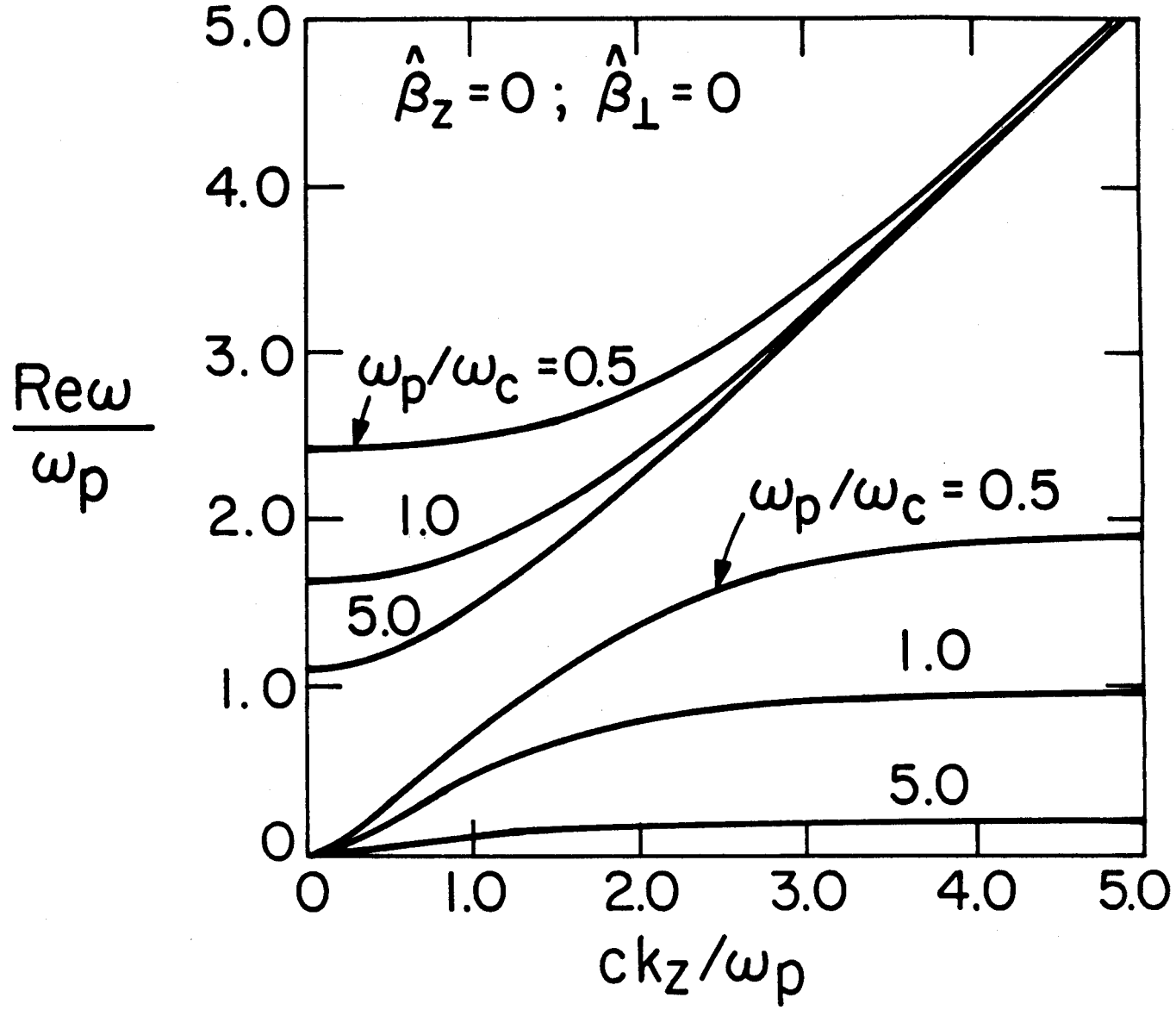
5.0
4.0
3.0
2.0
1.0
0
Reω / ωp
$\hat{\beta}_z = 0$; $\hat{\beta}_\perp = 0$
ω_p/ω_c =0.5
1.0
5.0
ω_p/ω_c = 0.5
1.0
5.0
0
1.0
2.0
3.0
4.0
5.0
ck_z/ω_p

Fig. 2

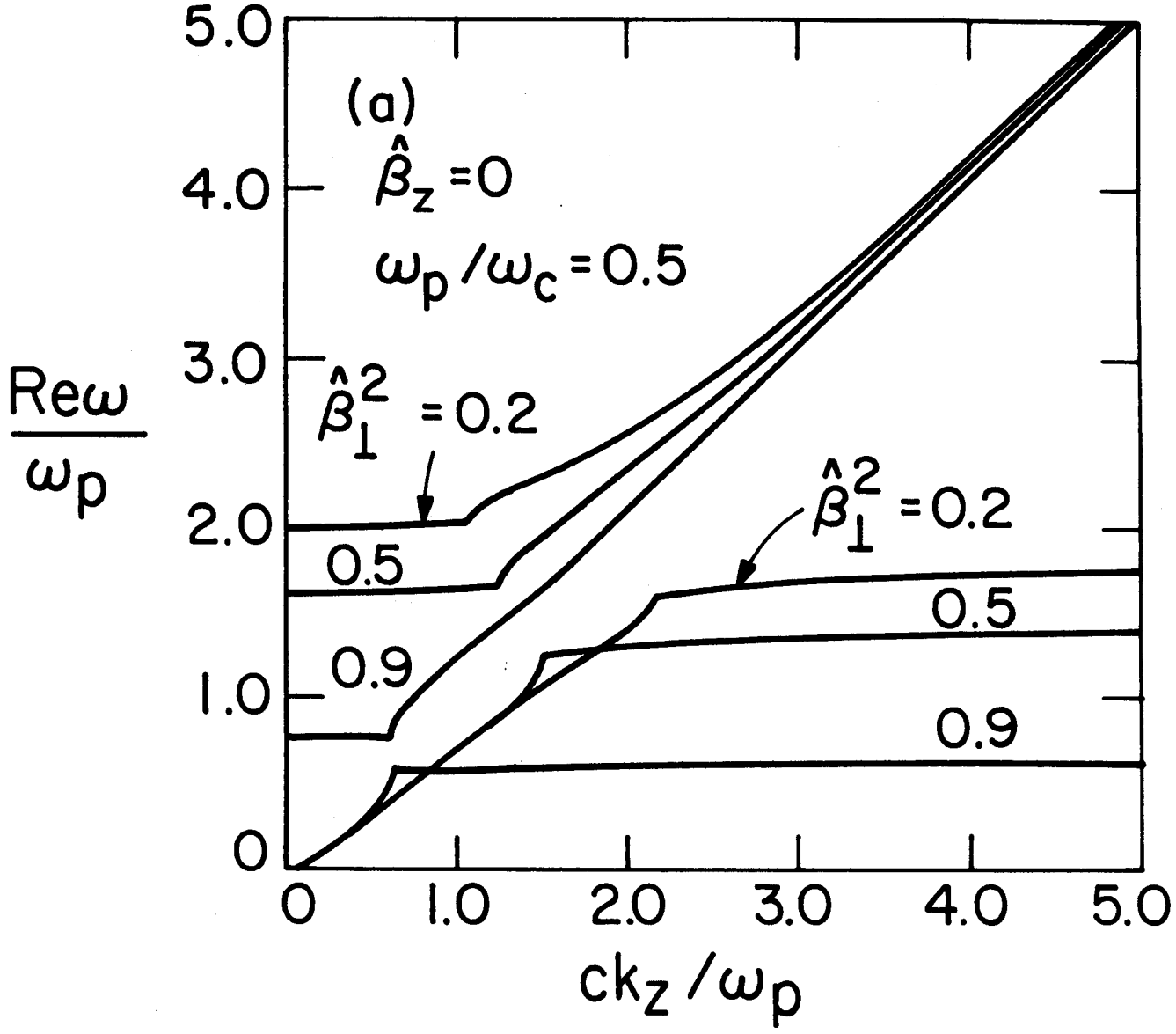
5.0
4.0
3.0
2.0
1.0
0
(a)
$\hat{\beta}_z = 0$
$\omega_p/\omega_c = 0.5$
$\hat{\beta}_\perp^2 = 0.2$
0.5
0.9
$\hat{\beta}_\perp^2 = 0.2$
0.5
0.9
$\frac{Re\omega}{\omega_p}$
0
1.0
2.0
3.0
4.0
5.0
ck_z/ω_p

Fig. 3(a)

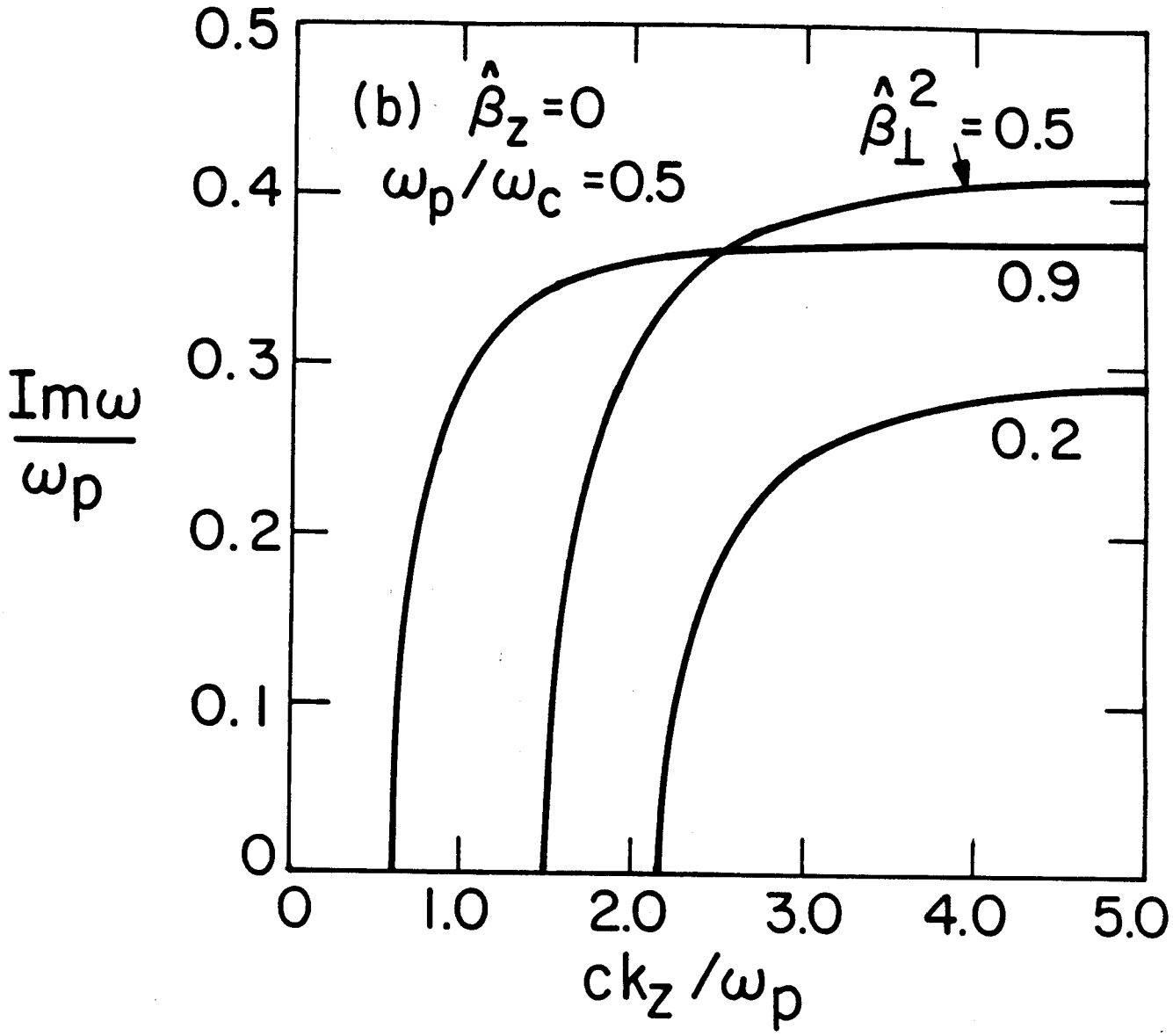
(b) $\hat{\beta}_z = 0$
$\omega_p/\omega_c = 0.5$
$\hat{\beta}_\perp^2 = 0.5$
0.9
0.2
$\frac{Im\omega}{\omega_p}$
ck_z/ω_p
0
0.1
0.2
0.3
0.4
0.5
1.0
2.0
3.0
4.0
5.0

Fig. 3(b)

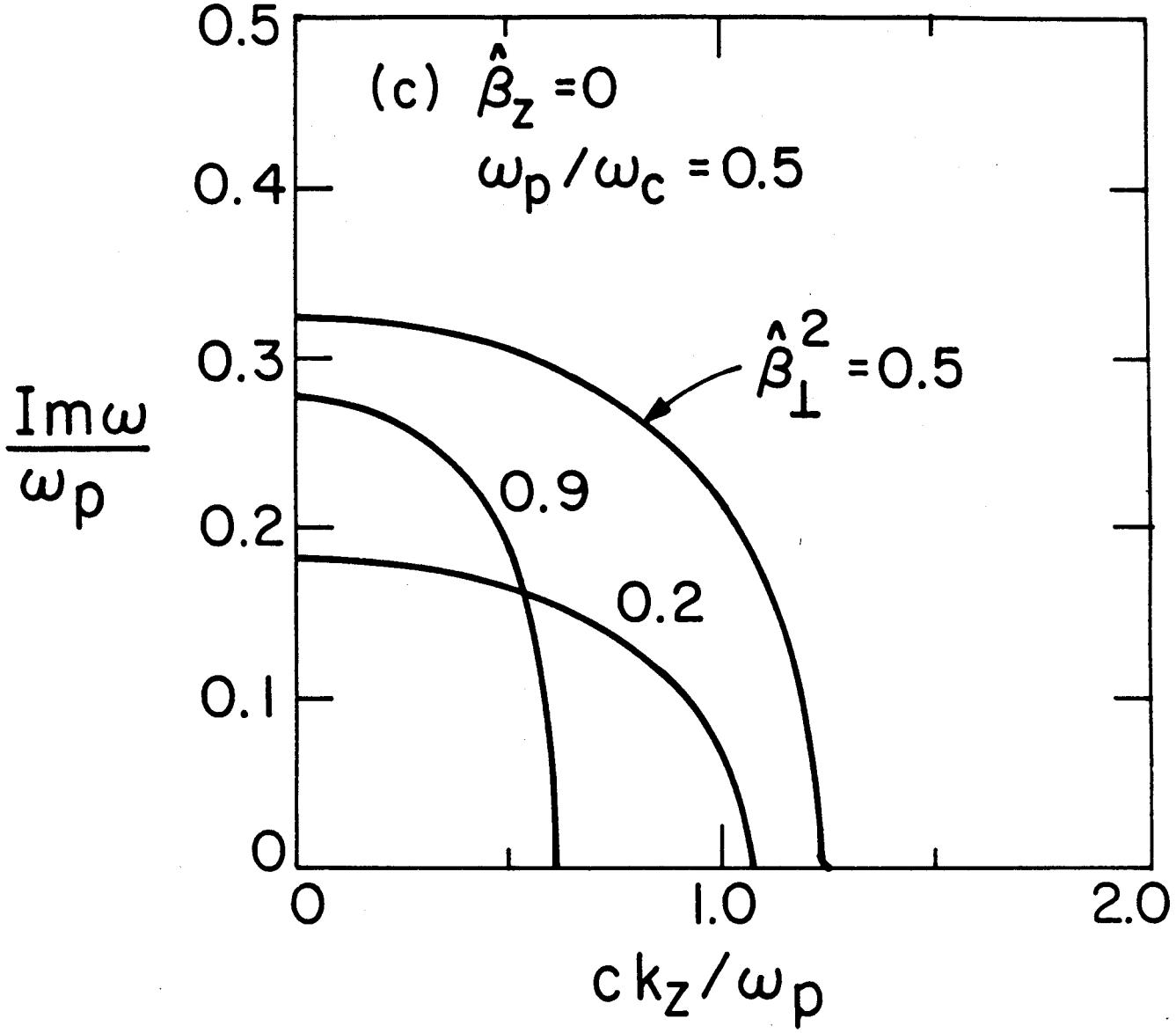
0.5
0.4
0.3
0.2
0.1
0
(c) $\hat{\beta}_z = 0$
$\omega_p / \omega_c = 0.5$
$\hat{\beta}_\perp^2 = 0.5$
0.9
0.2
$\frac{Im\omega}{\omega_p}$
0
1.0
2.0
ck_z/ω_p

Fig. 3(c)

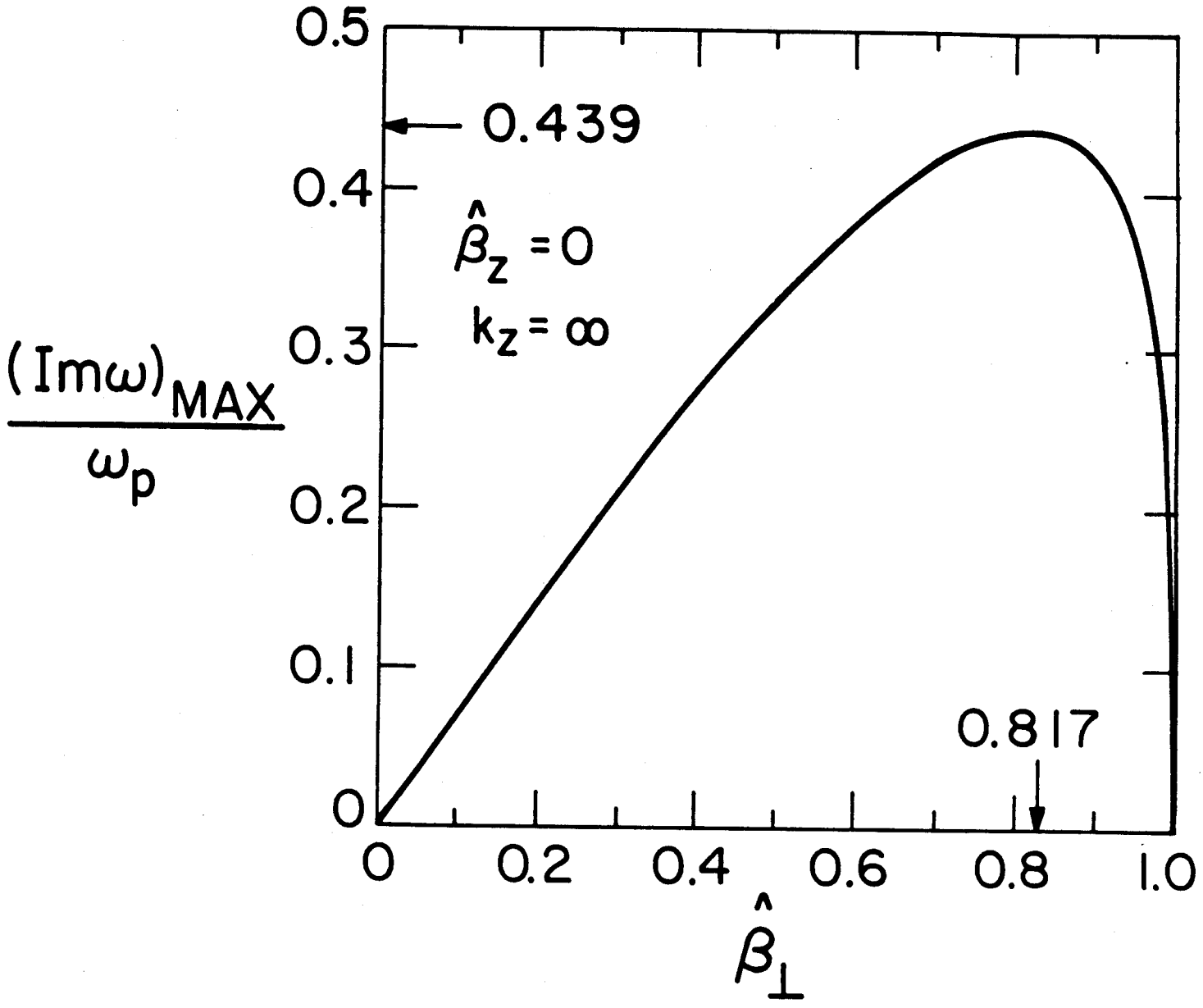
0.5
0.4
0.3
0.2
0.1
0
0.439
$\hat{\beta}_z = 0$
$k_z = \infty$
$\frac{(Im\omega)_{MAX}}{\omega_p}$
0.817
0
0.2
0.4
0.6
0.8
1.0
$\hat{\beta}_\perp$

Fig. 4

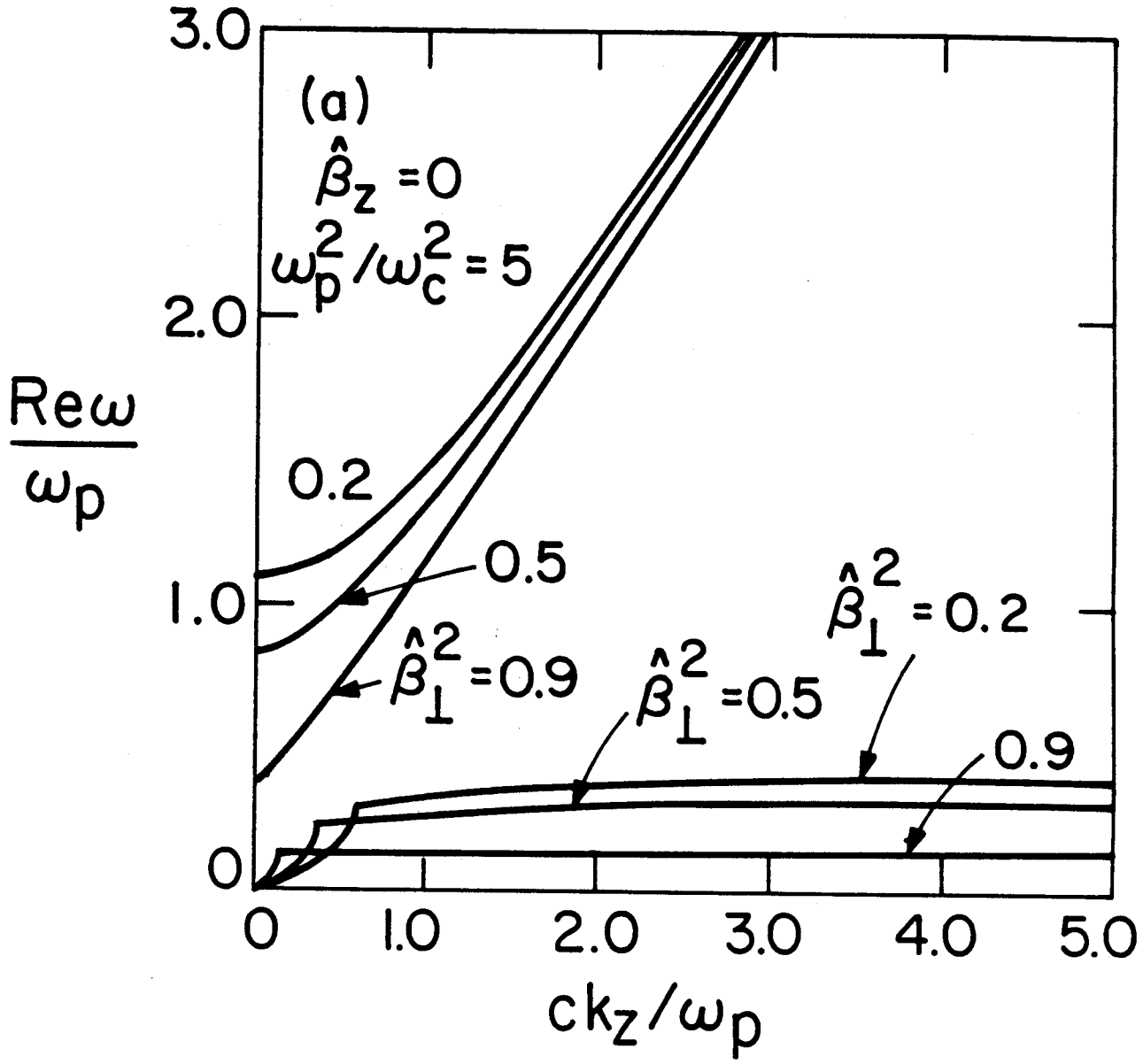
3.0
2.0
1.0
0
(a)
$\hat{\beta}_z = 0$
$\omega_p^2/\omega_c^2 = 5$
0.2
0.5
$\hat{\beta}_\perp^2 = 0.9$
$\hat{\beta}_\perp^2 = 0.5$
$\hat{\beta}_\perp^2 = 0.2$
0.9
$\frac{Re\omega}{\omega_p}$
0
1.0
2.0
3.0
4.0
5.0
ck_z/ω_p

Fig. 5(a)

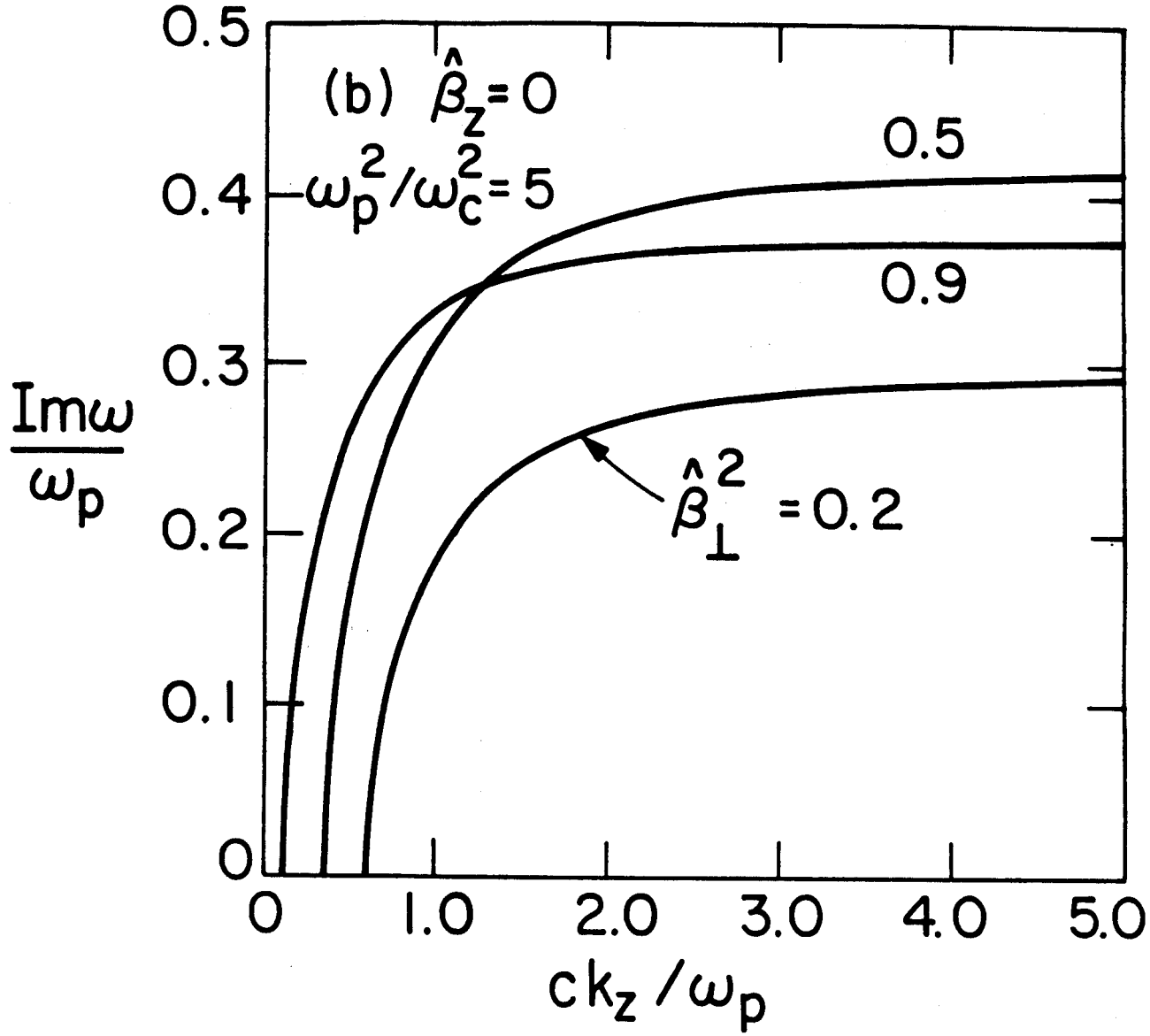
0.5
0.4
0.3
0.2
0.1
0
(b) $\hat{\beta}_z = 0$
$\omega_p^2/\omega_c^2 = 5$
0.5
0.9
$\hat{\beta}_\perp^2 = 0.2$
$\frac{Im\omega}{\omega_p}$
0
1.0
2.0
3.0
4.0
5.0
ck_z/ω_p

Fig. 5(b)

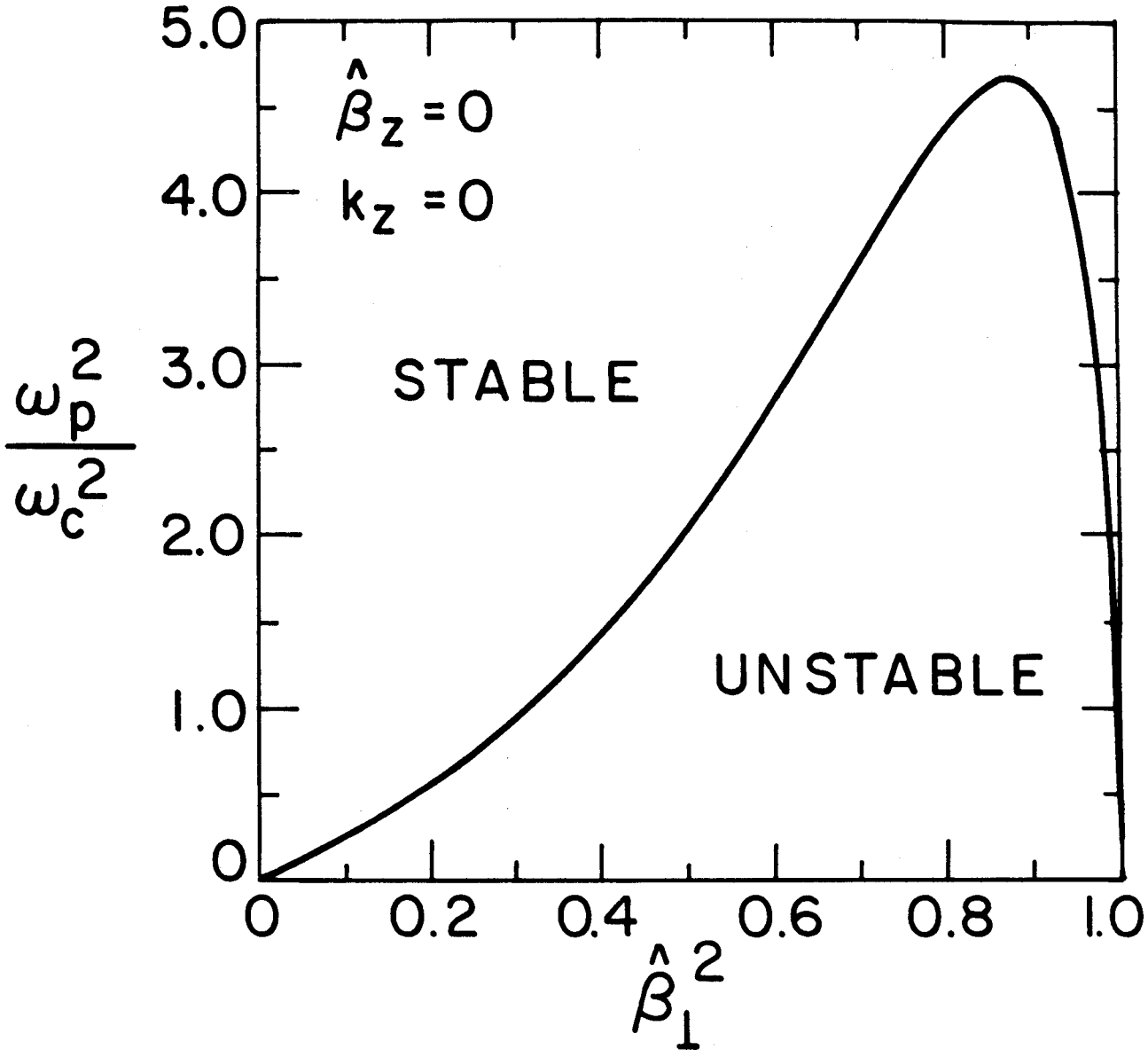
5.0
4.0
3.0
2.0
1.0
0
$\hat{\beta}_z = 0$
$k_z = 0$
STABLE
UNSTABLE
$\frac{\omega_p^2}{\omega_c^2}$
0
0.2
0.4
0.6
0.8
1.0
$\hat{\beta}_\perp^2$

Fig. 6

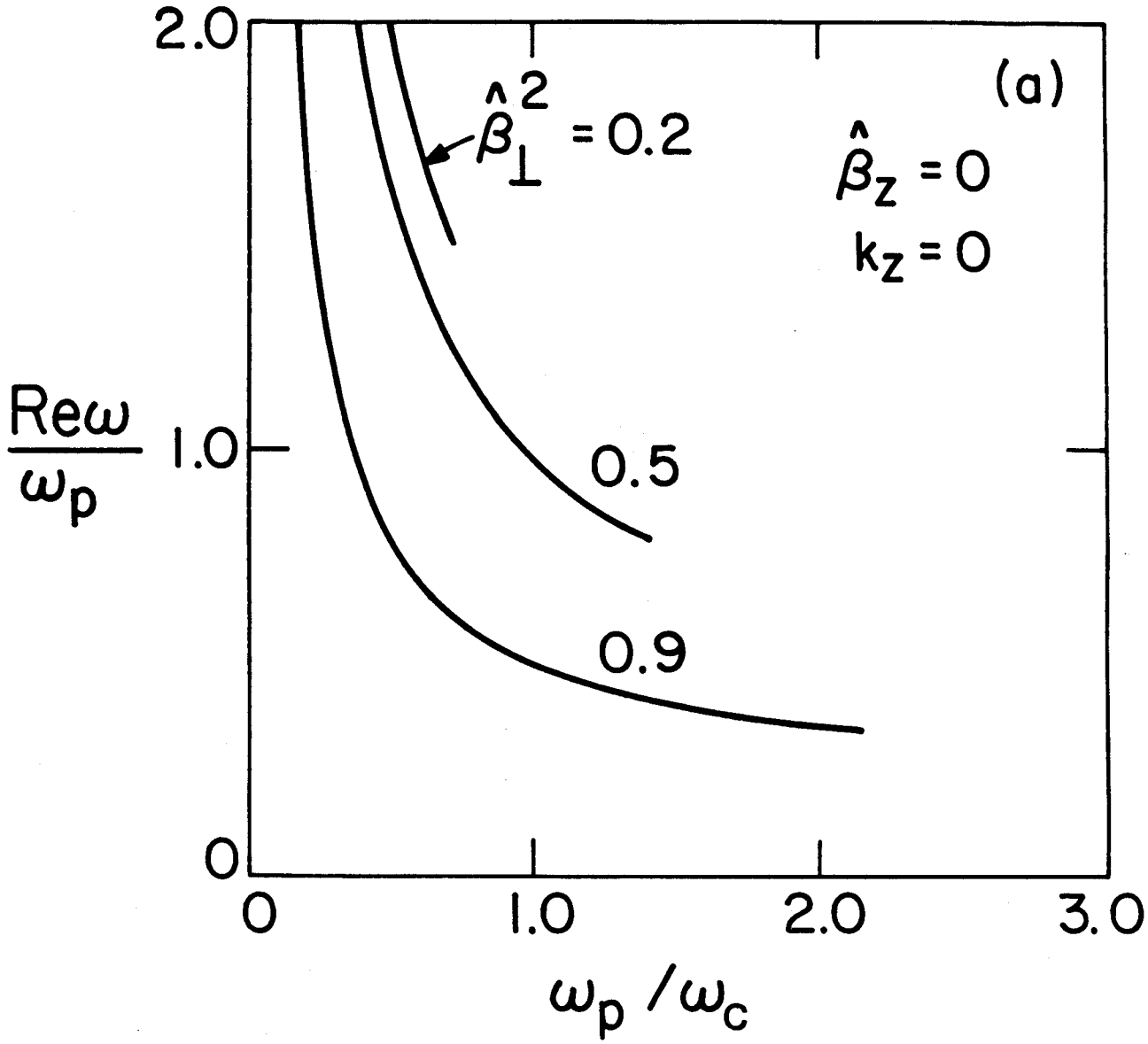

Fig. 7(a)

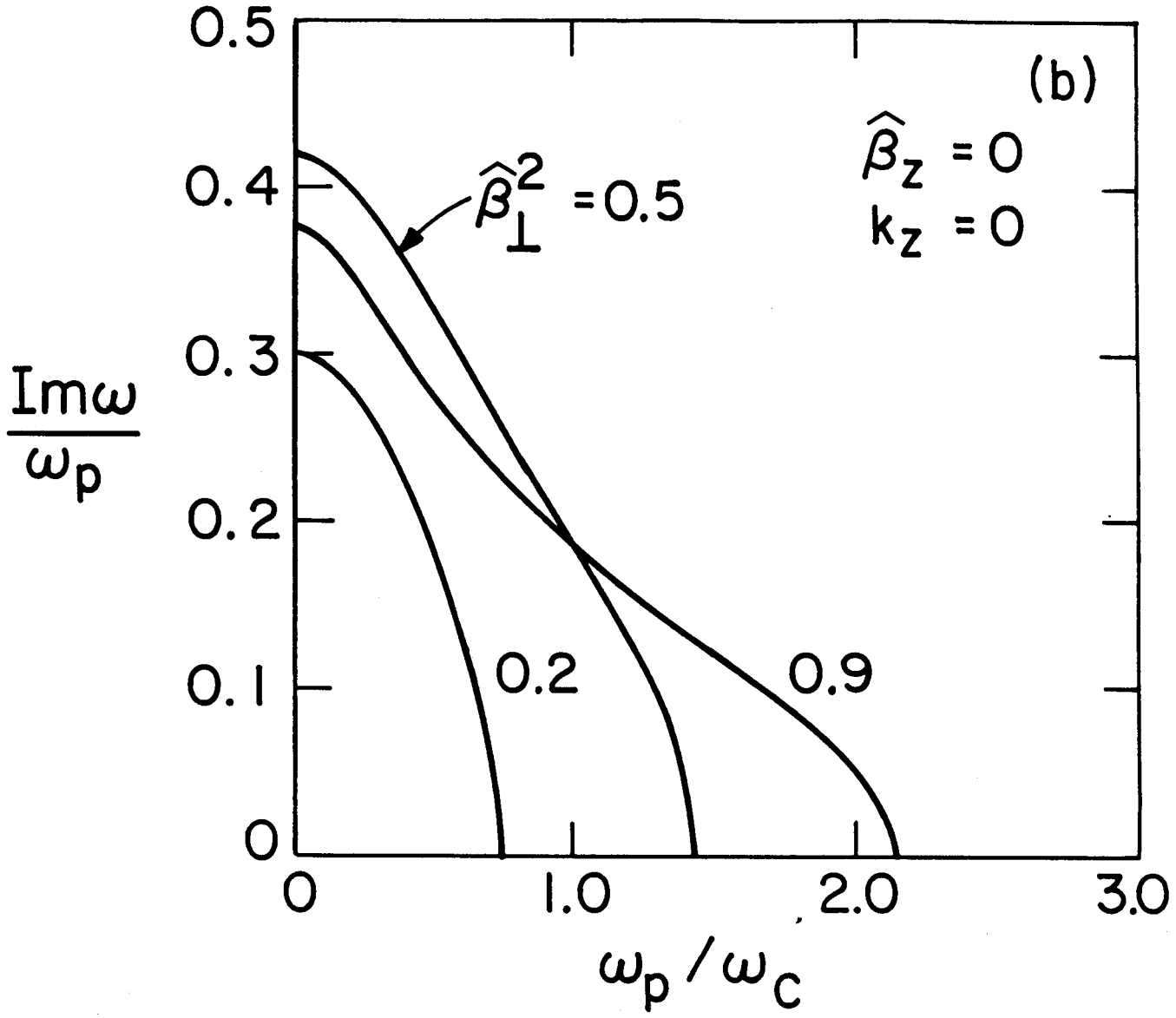

Fig. 7(b)

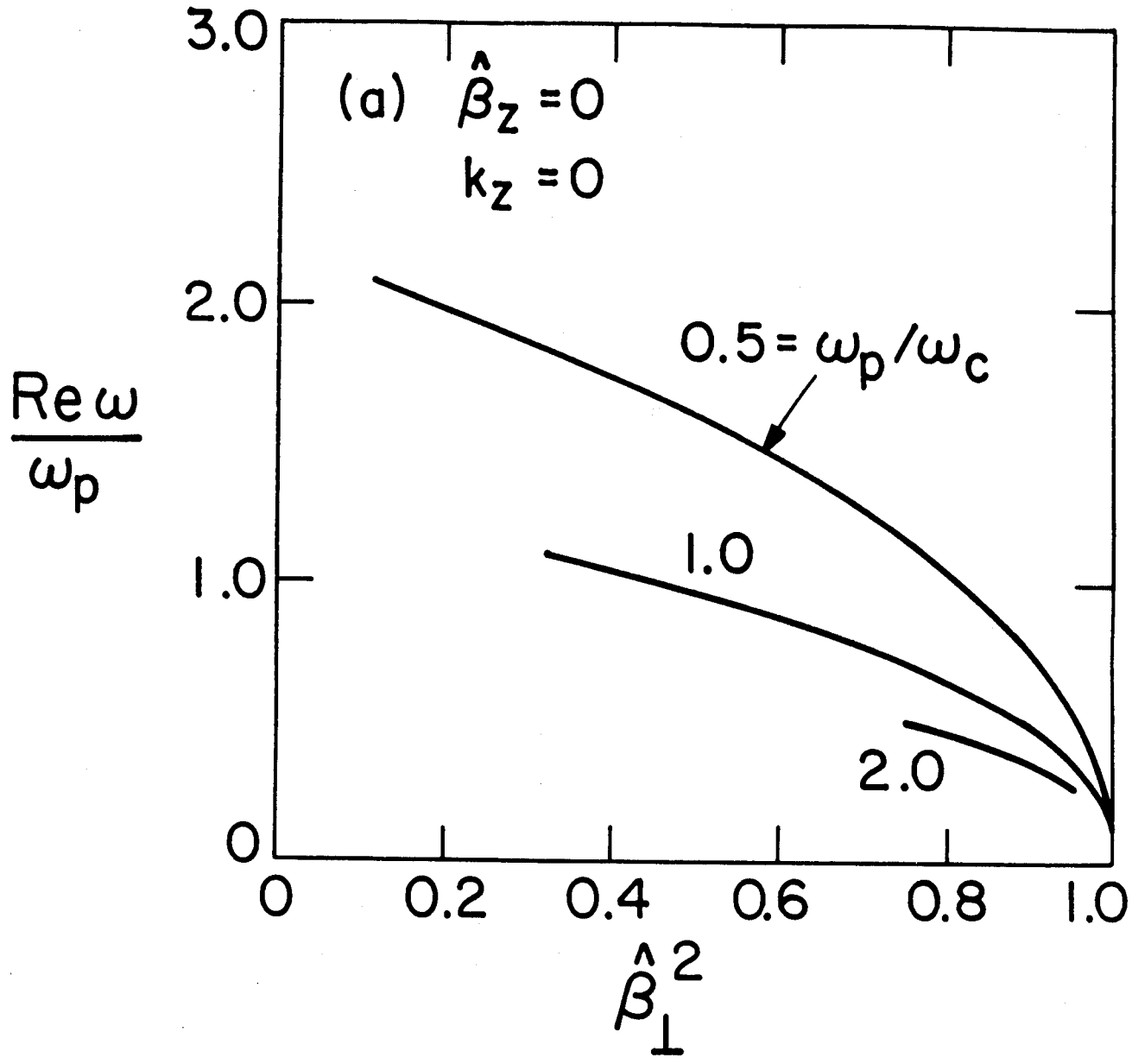
3.0
2.0
1.0
0
(a) $\hat{\beta}_z = 0$
$k_z = 0$
0.5 = ω_p/ω_c
1.0
2.0
$\frac{Re\,\omega}{\omega_p}$
0
0.2
0.4
0.6
0.8
1.0
$\hat{\beta}_\perp^2$

Fig. 8(a)

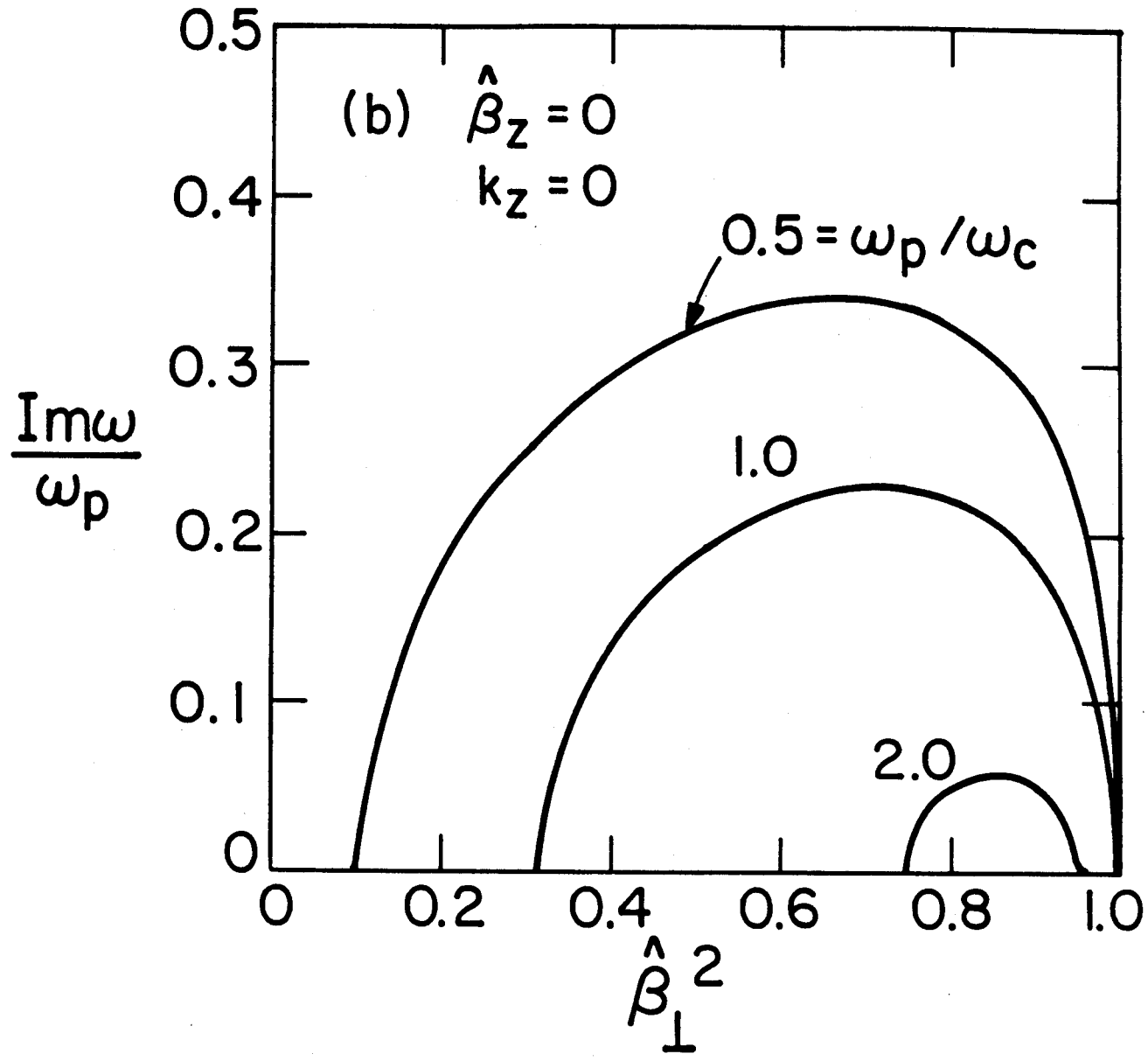
0.5
0.4
0.3
0.2
0.1
0
(b) $\hat{\beta}_z = 0$
$k_z = 0$
$0.5 = \omega_p / \omega_c$
1.0
2.0
$\frac{Im\omega}{\omega_p}$
0
0.2
0.4
0.6
0.8
1.0
$\hat{\beta}_\perp^2$

Fig. 8(b)

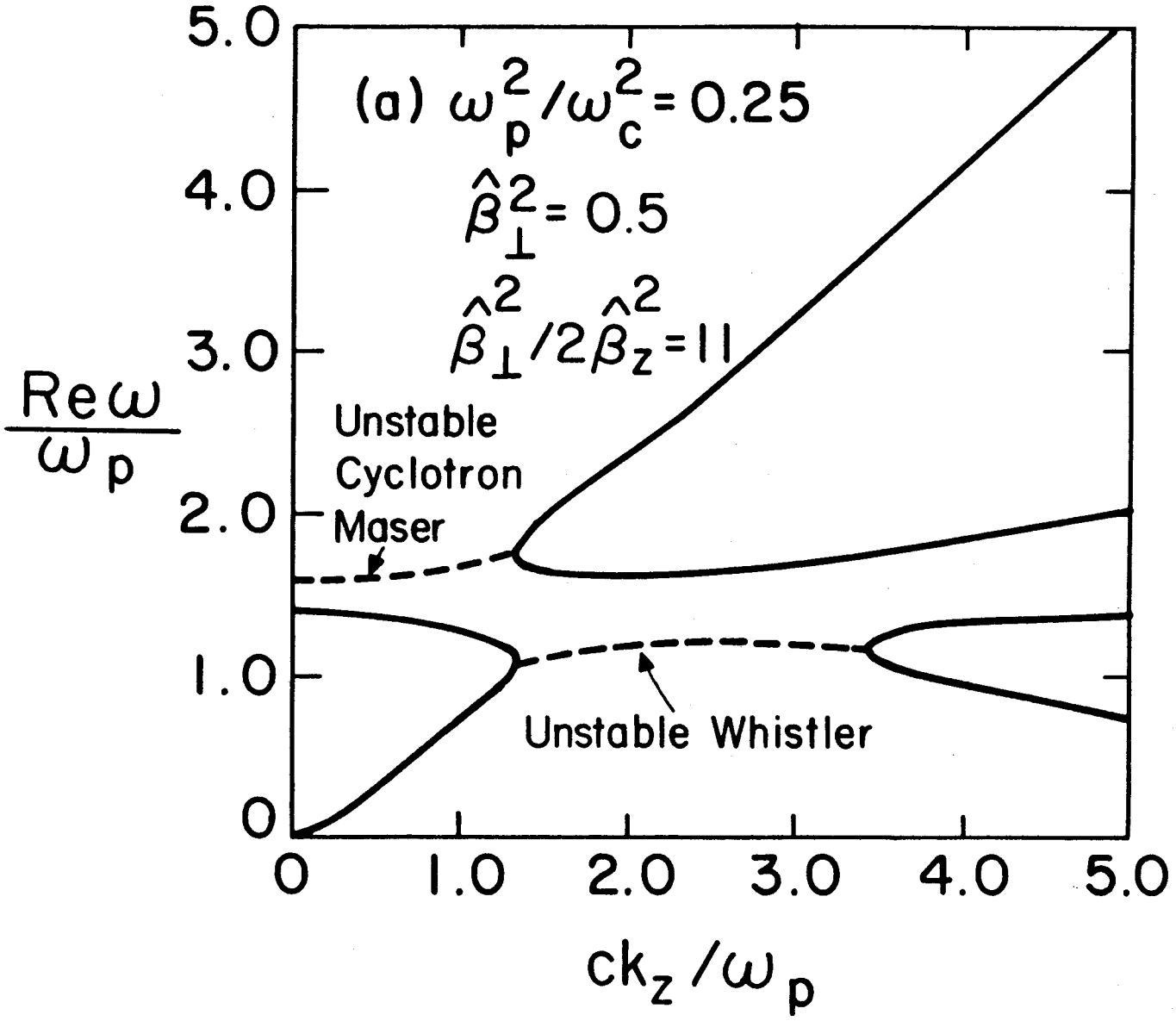
(a) $\omega_p^2/\omega_c^2 = 0.25$
$\hat{\beta}_\perp^2 = 0.5$
$\hat{\beta}_\perp^2/2\hat{\beta}_z^2 = 11$
Unstable Cyclotron Maser
Unstable Whistler
$\frac{Re\,\omega}{\omega_p}$
ck_z/ω_p
0
1.0
2.0
3.0
4.0
5.0

Fig. 9(a)

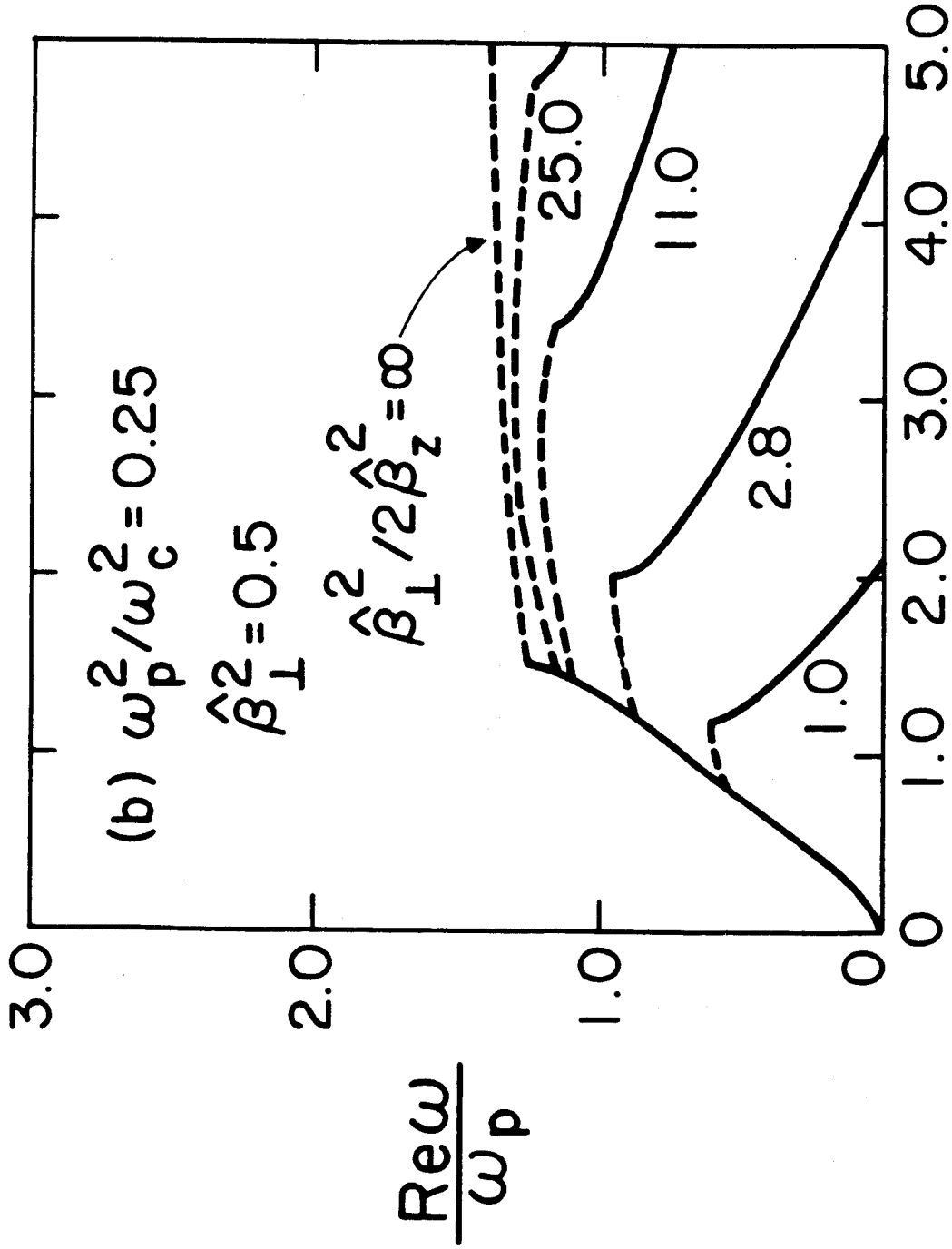
(b) $\omega_p^2/\omega_c^2 = 0.25$
$\hat{\beta}_\perp^2 = 0.5$
$\hat{\beta}_\perp^2/2\hat{\beta}_z^2 = \infty$
25.0
11.0
2.8
1.0
$\frac{Re\omega}{\omega_p}$
ck_z/ω_p
0
1.0
2.0
3.0
4.0
5.0

Fig. 9(b)

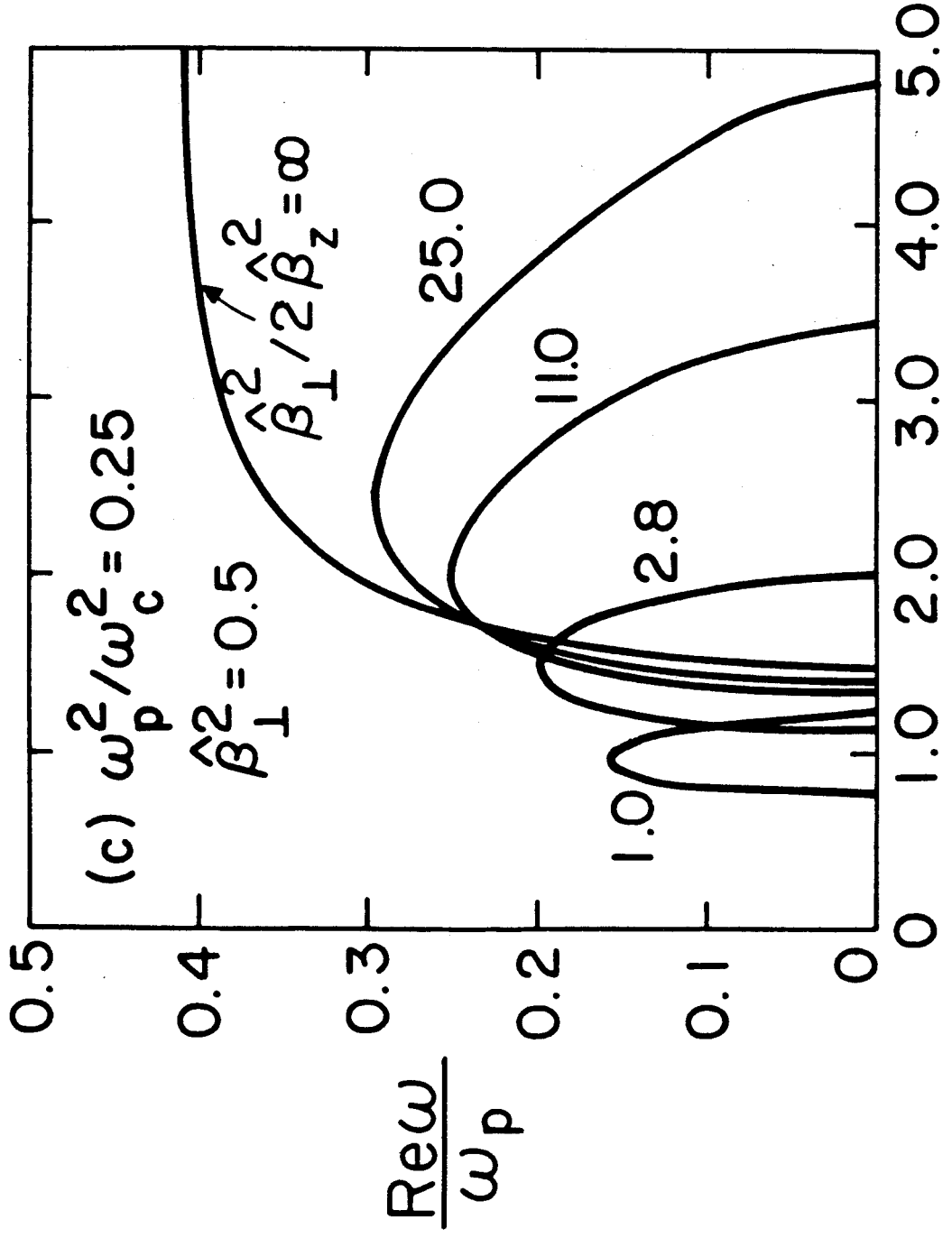
(c) $\omega_p^2/\omega_c^2 = 0.25$
$\hat{\beta}_\perp^2 = 0.5$
$\hat{\beta}_\perp^2/2\hat{\beta}_z^2 = \infty$
25.0
11.0
2.8
1.0
$\frac{Re\omega}{\omega_p}$
ck_z/ω_p
0
0.1
0.2
0.3
0.4
0.5
1.0
2.0
3.0
4.0
5.0

Fig. 9(c)

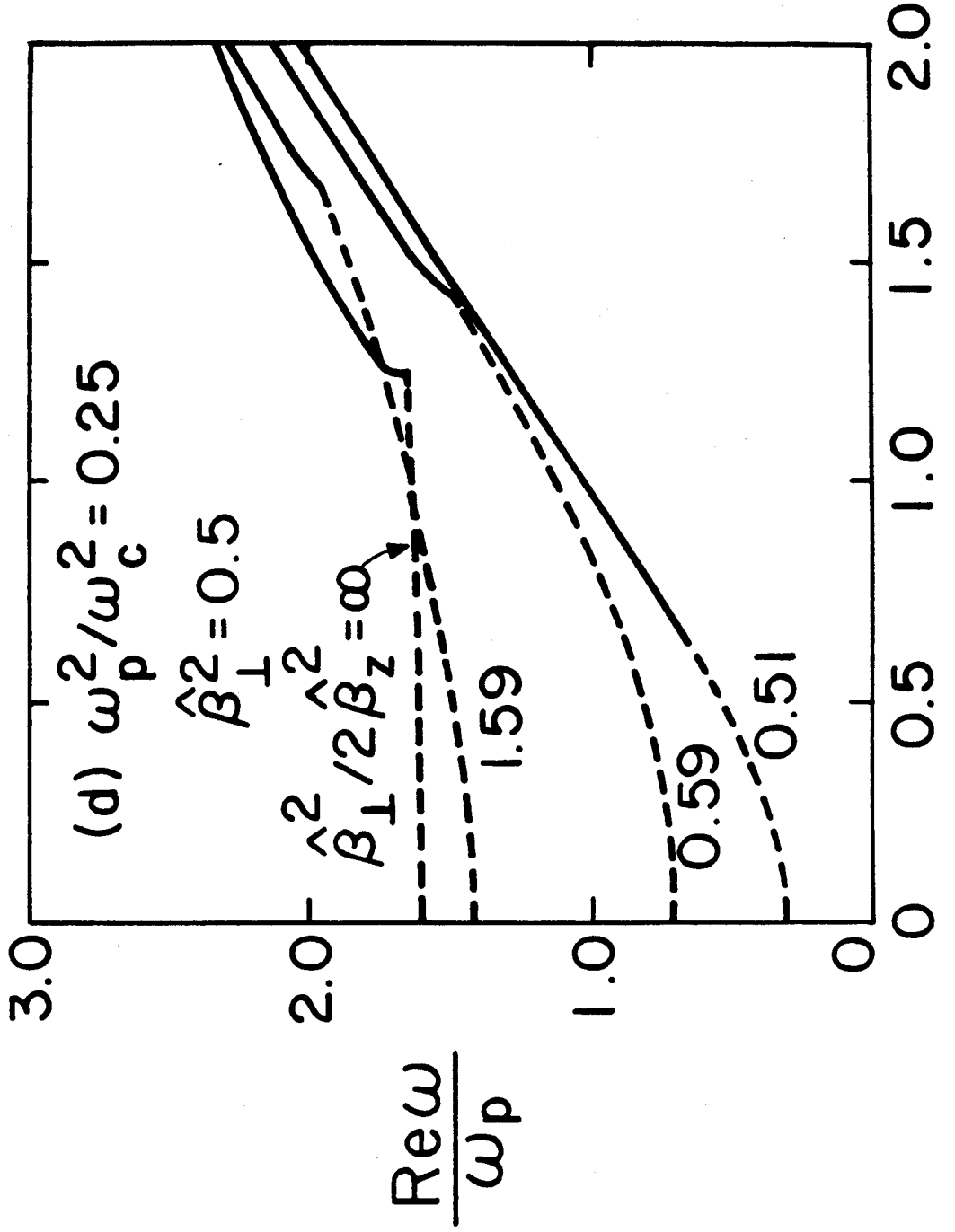
(d) $\omega_p^2/\omega_c^2 = 0.25$
$\hat{\beta}_\perp^2 = 0.5$
$\hat{\beta}_\perp^2/2\hat{\beta}_z^2 = \infty$
1.59
0.59
0.51
$\frac{Re\omega}{\omega_p}$
ck_z/ω_p
3.0
2.0
1.0
0
0.5
1.0
1.5
2.0

Fig. 9(d)

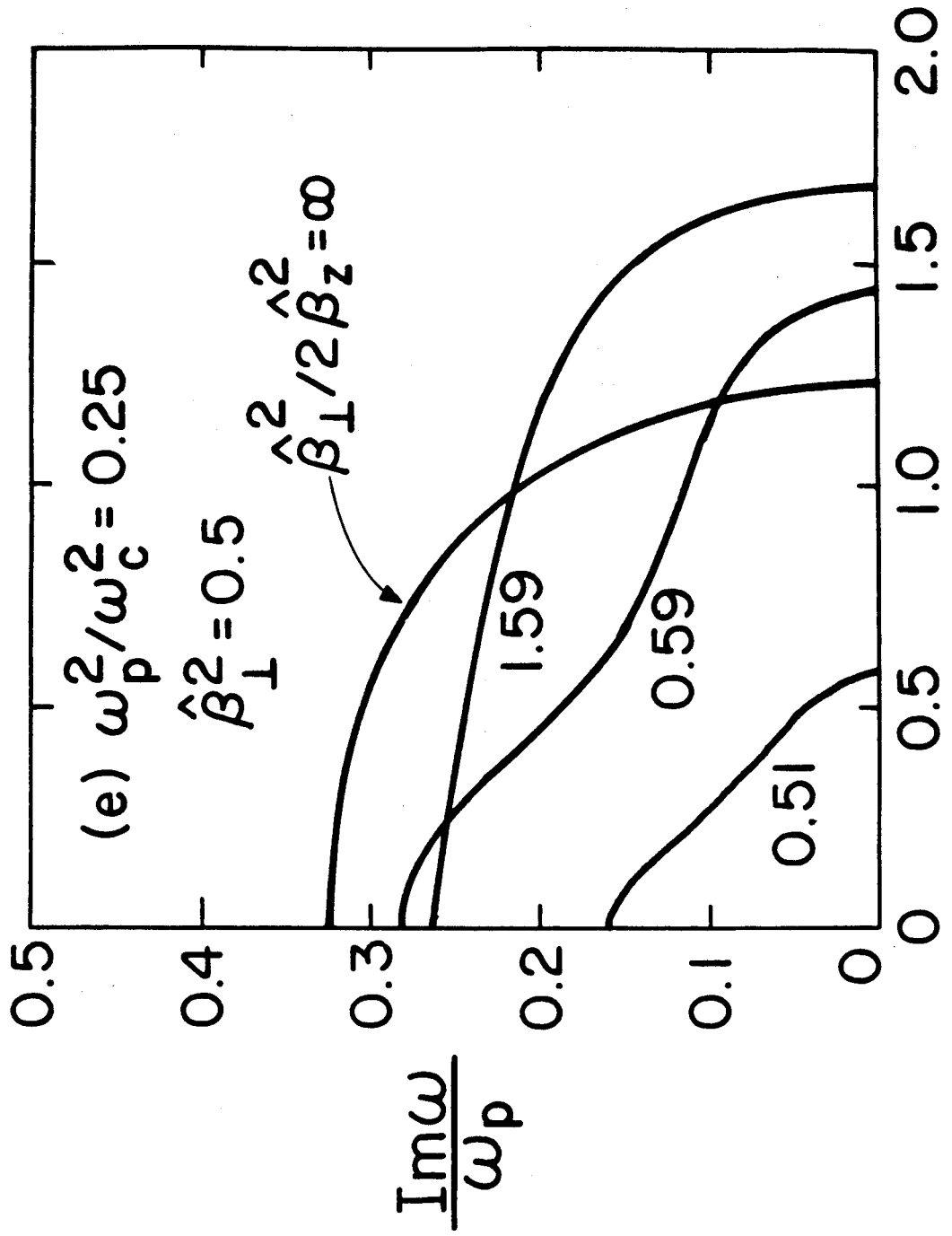
(e) $\omega_p^2/\omega_c^2 = 0.25$
$\hat{\beta}_\perp^2 = 0.5$
$\hat{\beta}_\perp^2/2\hat{\beta}_z^2 = \infty$
1.59
0.59
0.51
$\frac{Im\omega}{\omega_p}$
ck_z/ω_p
0.5
0.4
0.3
0.2
0.1
0
0
0.5
1.0
1.5
2.0

Fig. 9(e)

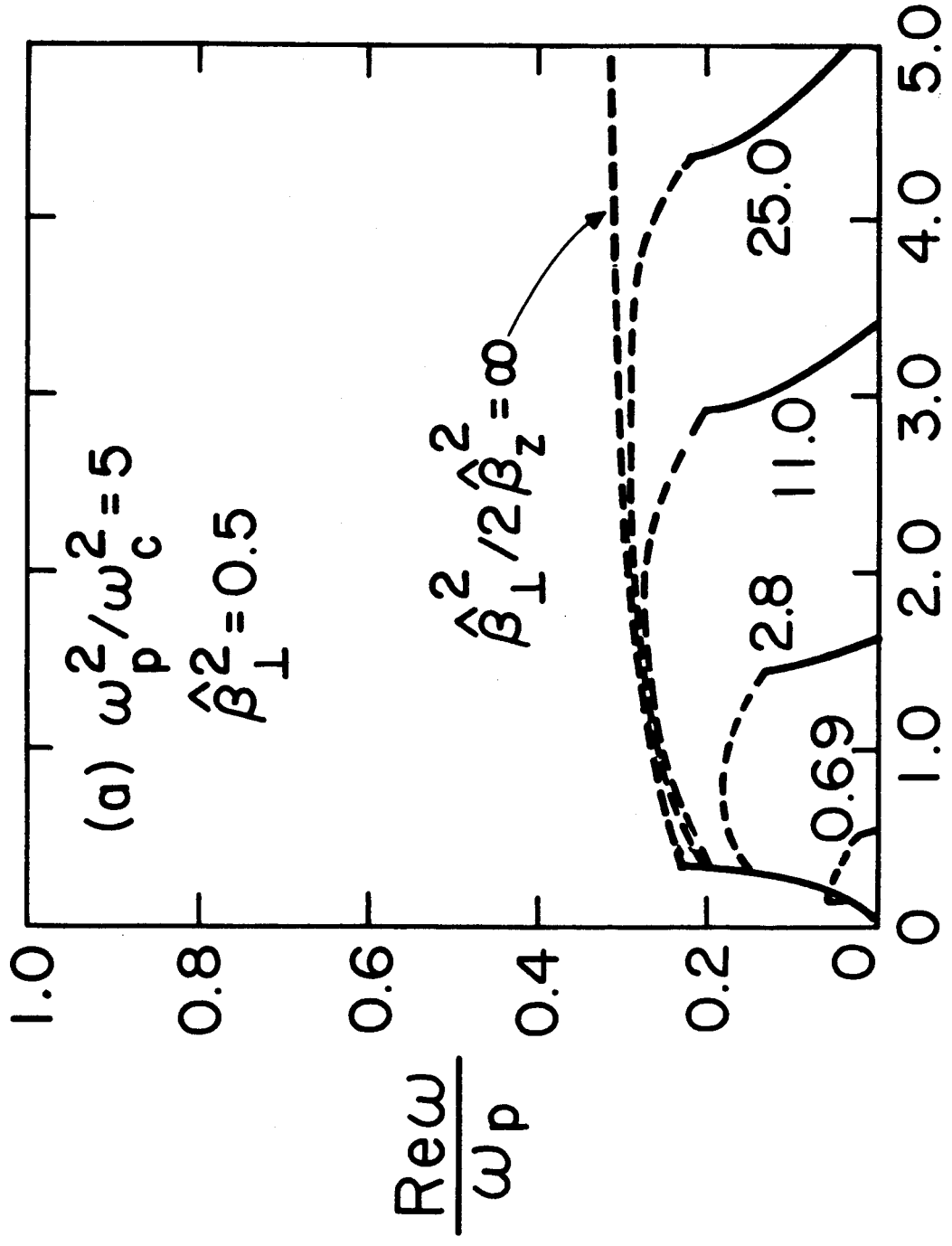
(a) $\omega_p^2/\omega_c^2=5$
$\hat{\beta}_\perp^2=0.5$
$\hat{\beta}_\perp^2/2\hat{\beta}_z^2=\infty$
25.0
11.0
2.8
0.69
$\frac{Re\omega}{\omega_p}$
ck_z/ω_p
0
0.2
0.4
0.6
0.8
1.0
1.0
2.0
3.0
4.0
5.0

Fig. 10(a)

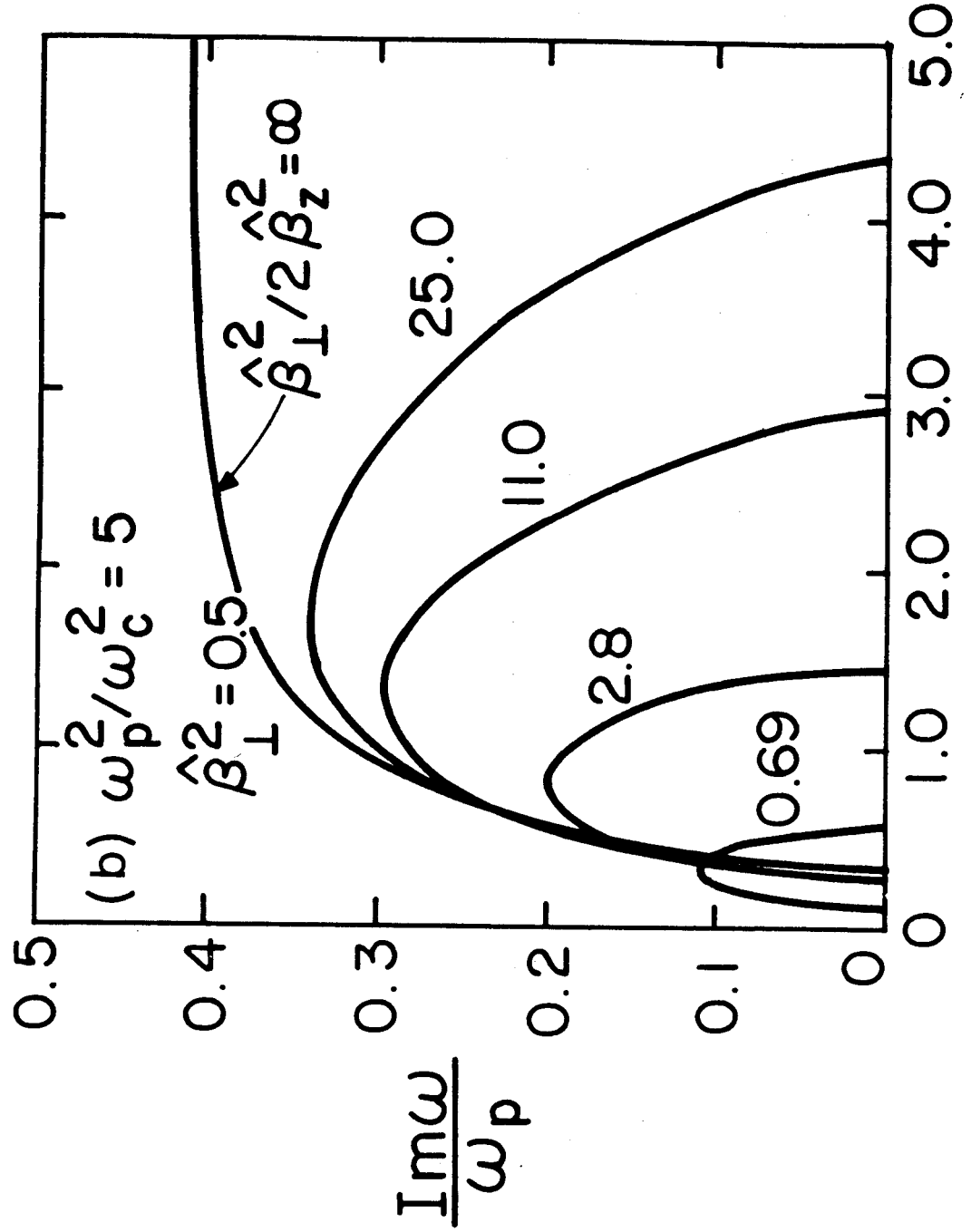
(b) $\omega_p^2/\omega_c^2 = 5$
$\hat{\beta}_\perp^2 = 0.5$
$\hat{\beta}_\perp^2/2\hat{\beta}_z^2 = \infty$
25.0
11.0
2.8
0.69
$\frac{Im\omega}{\omega_p}$
ck_z/ω_p
0
0.1
0.2
0.3
0.4
0.5
1.0
2.0
3.0
4.0
5.0

Fig. 10(b)

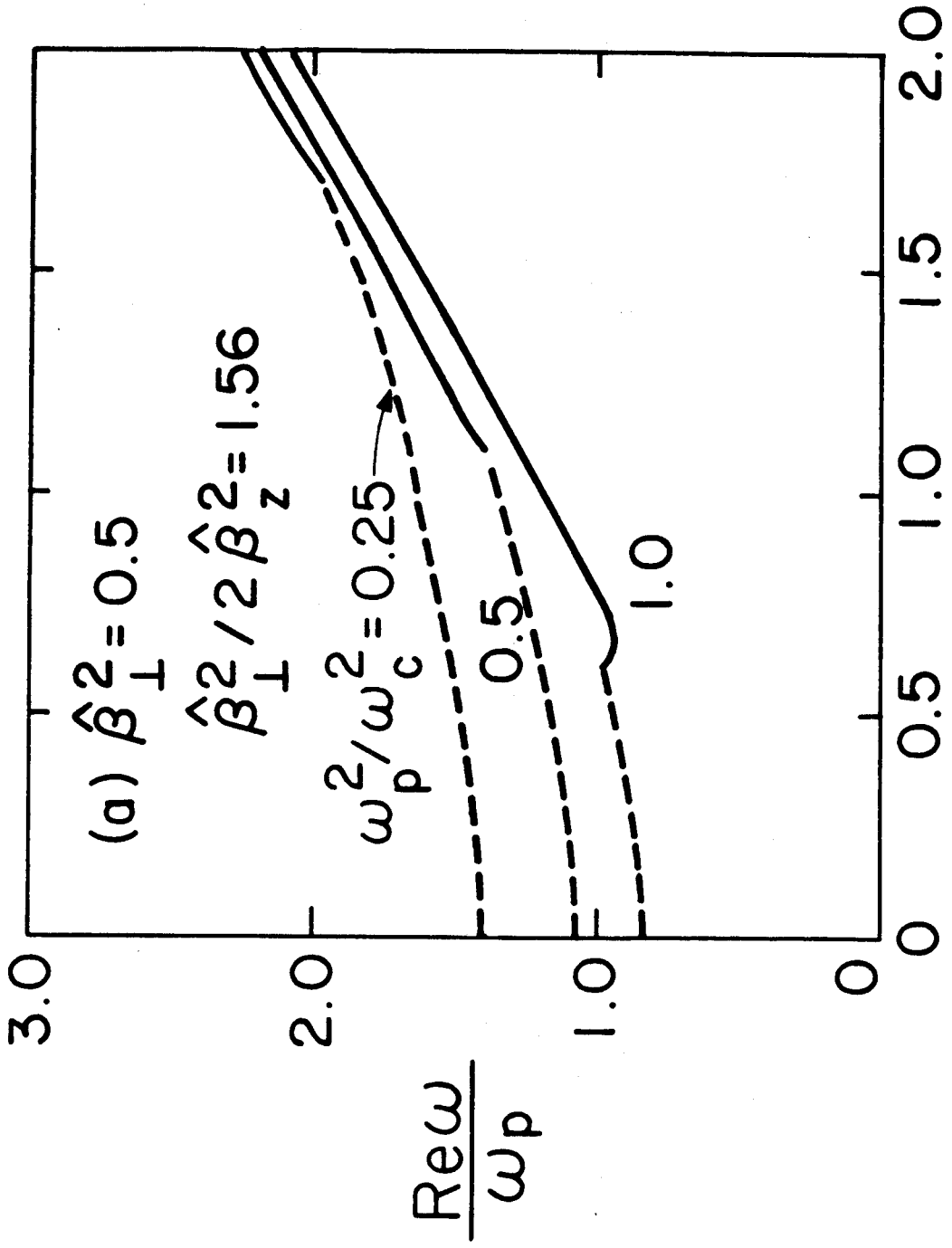
(a) $\hat{\beta}_\perp^2 = 0.5$
$\hat{\beta}_\perp^2 / 2\hat{\beta}_z^2 = 1.56$
$\omega_p^2/\omega_c^2 = 0.25$
0.5
1.0
$\frac{Re\omega}{\omega_p}$
ck_z/ω_p
0
1.0
2.0
3.0
0.5
1.0
1.5
2.0

Fig. 11(a)

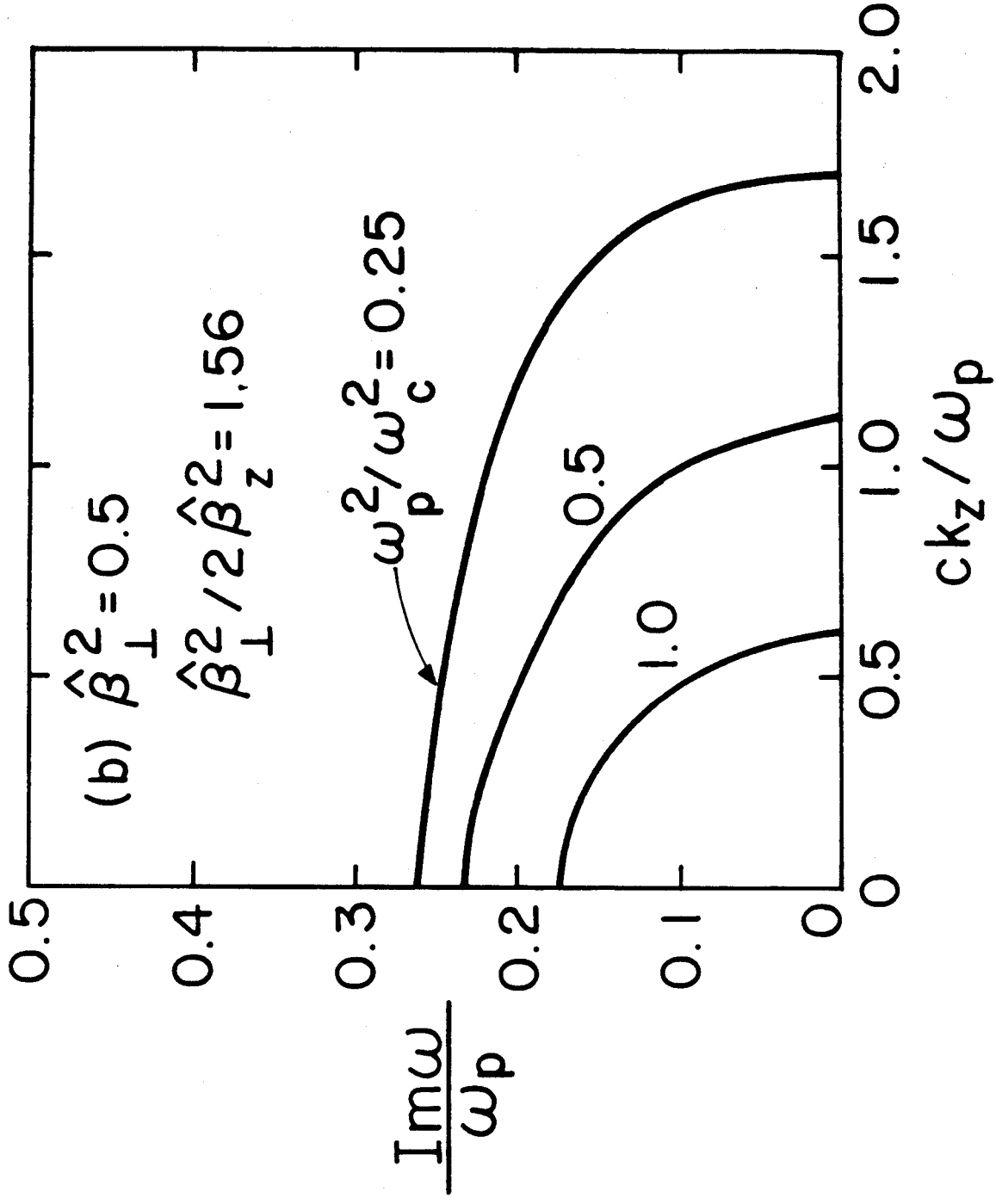
(b) $\hat{\beta}_\perp^2 = 0.5$
$\hat{\beta}_\perp^2 / 2\hat{\beta}_z^2 = 1.56$
$\omega_p^2/\omega_c^2 = 0.25$
0.5
1.0
$\frac{Im\omega}{\omega_p}$
0.5
0.4
0.3
0.2
0.1
0
0
0.5
1.0
1.5
2.0
ck_z/ω_p

Fig. 11(b)

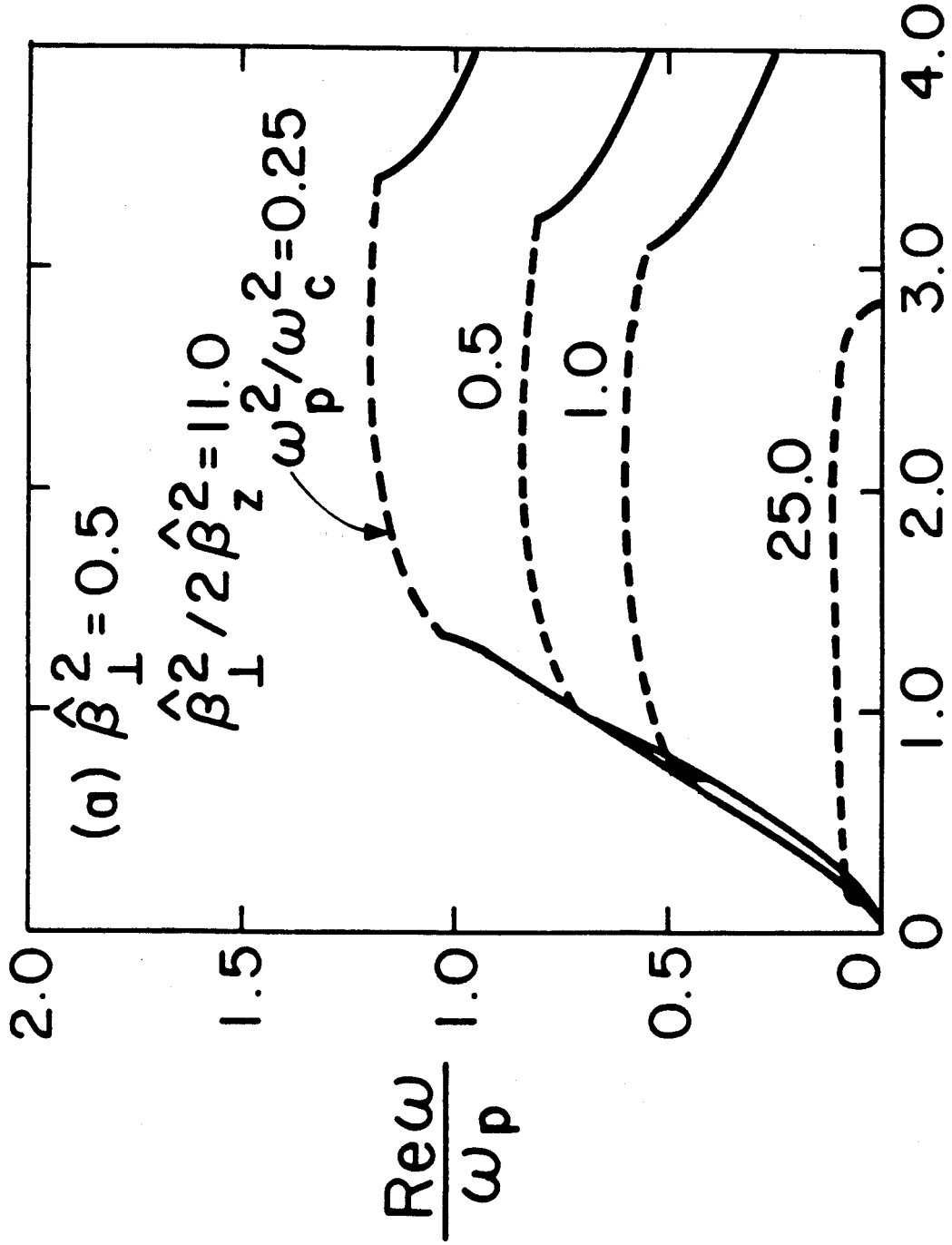
(a) $\hat{\beta}_\perp^2 = 0.5$
$\hat{\beta}_\perp^2 / 2\hat{\beta}_z^2 = 11.0$
$\omega_p^2/\omega_c^2 = 0.25$
0.5
1.0
25.0
$\frac{Re\omega}{\omega_p}$
ck_z/ω_p
0
0.5
1.0
1.5
2.0
1.0
2.0
3.0
4.0

Fig. 12(a)

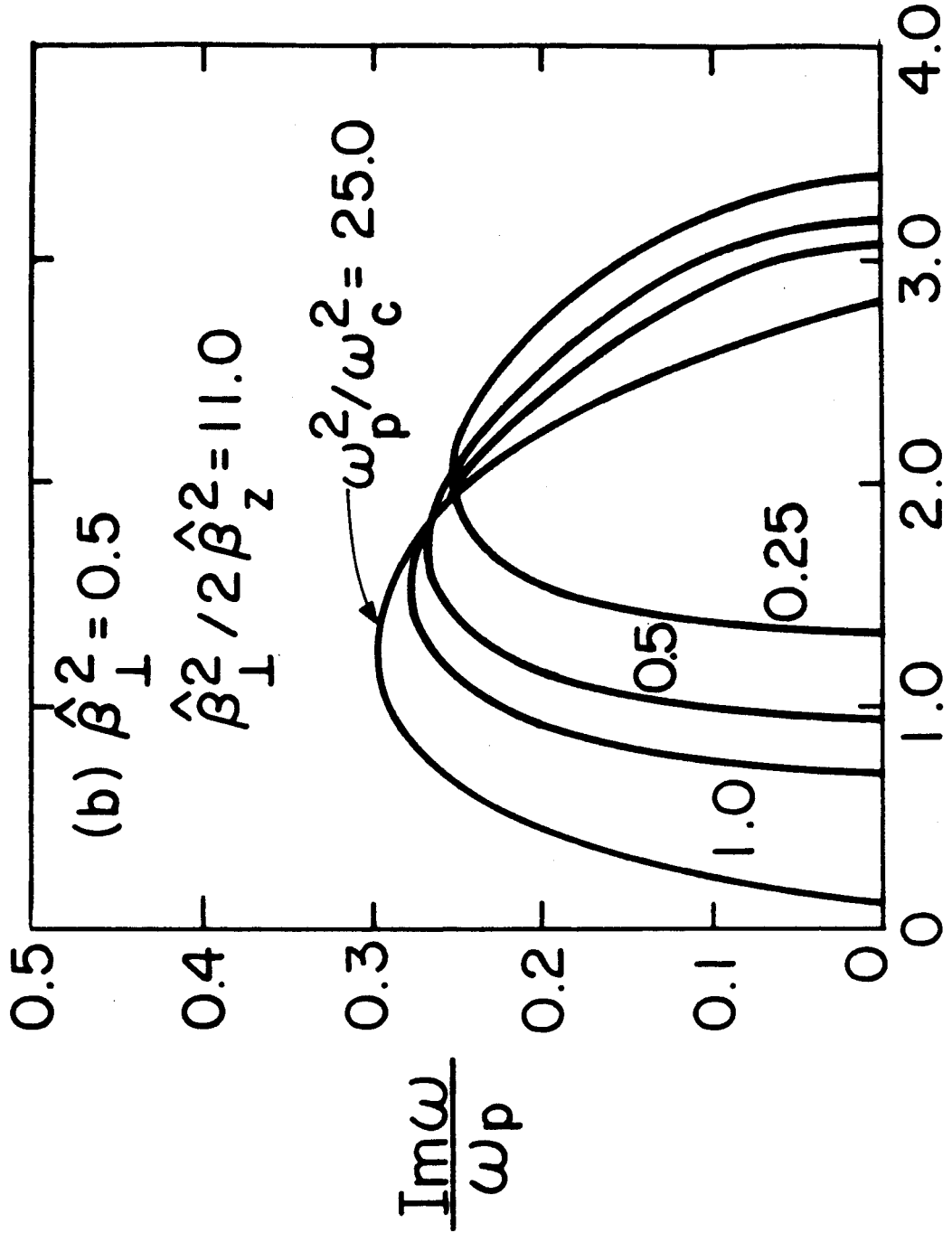
(b) $\hat{\beta}_\perp^2 = 0.5$
$\hat{\beta}_\perp^2 / 2\hat{\beta}_z^2 = 11.0$
$\omega_p^2/\omega_c^2 = 25.0$
1.0
0.5
0.25
0
0.1
0.2
0.3
0.4
0.5
1.0
2.0
3.0
4.0
$\frac{Im\omega}{\omega_p}$
ck_z/ω_p

Fig. 12(b)

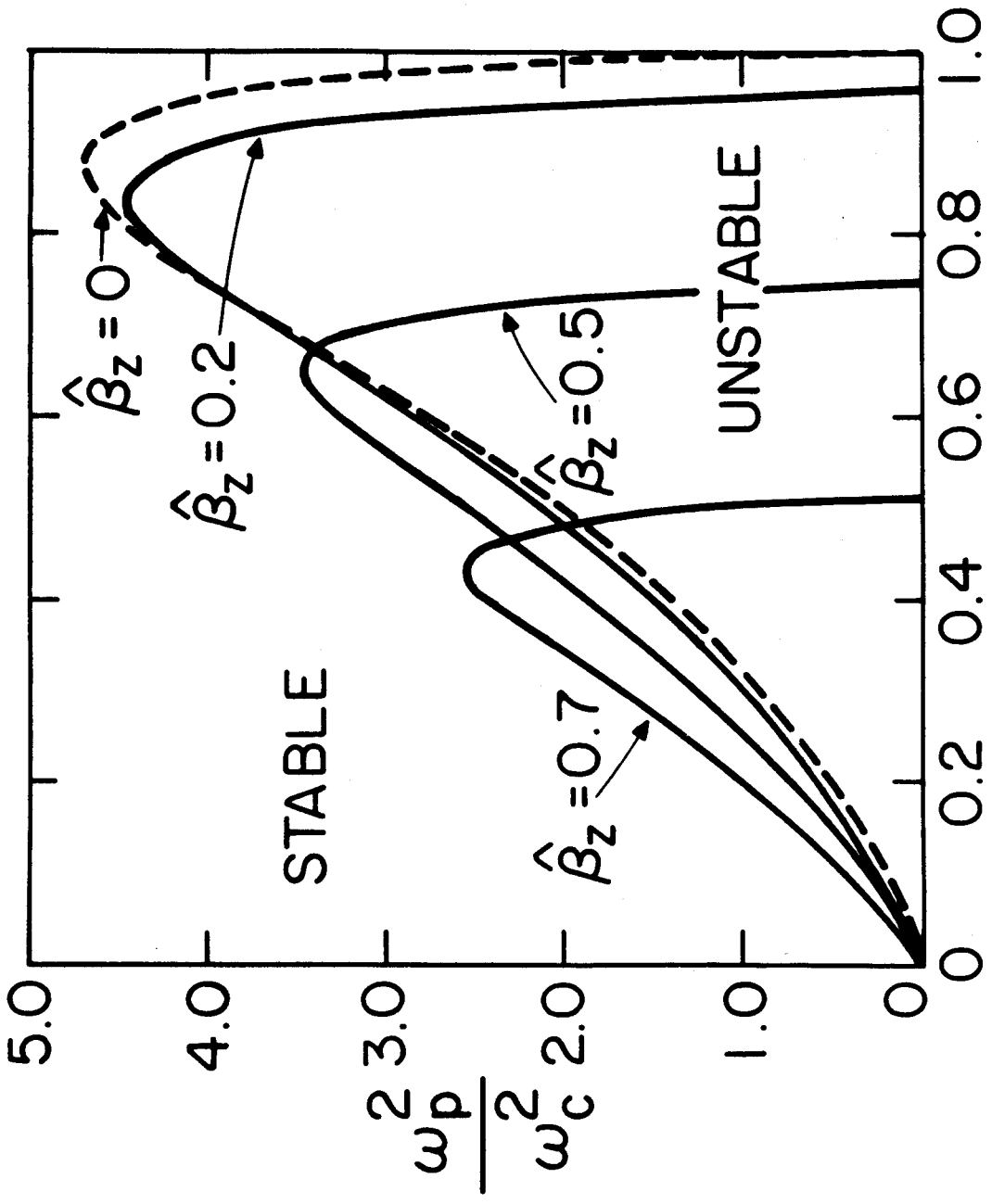
5.0
4.0
3.0
2.0
1.0
0
$\frac{\omega_p^2}{\omega_c^2}$
0
0.2
0.4
0.6
0.8
1.0
$\hat{\beta}_\perp^2$
STABLE
UNSTABLE
$\hat{\beta}_z = 0$
$\hat{\beta}_z = 0.2$
$\hat{\beta}_z = 0.5$
$\hat{\beta}_z = 0.7$

Fig. 13

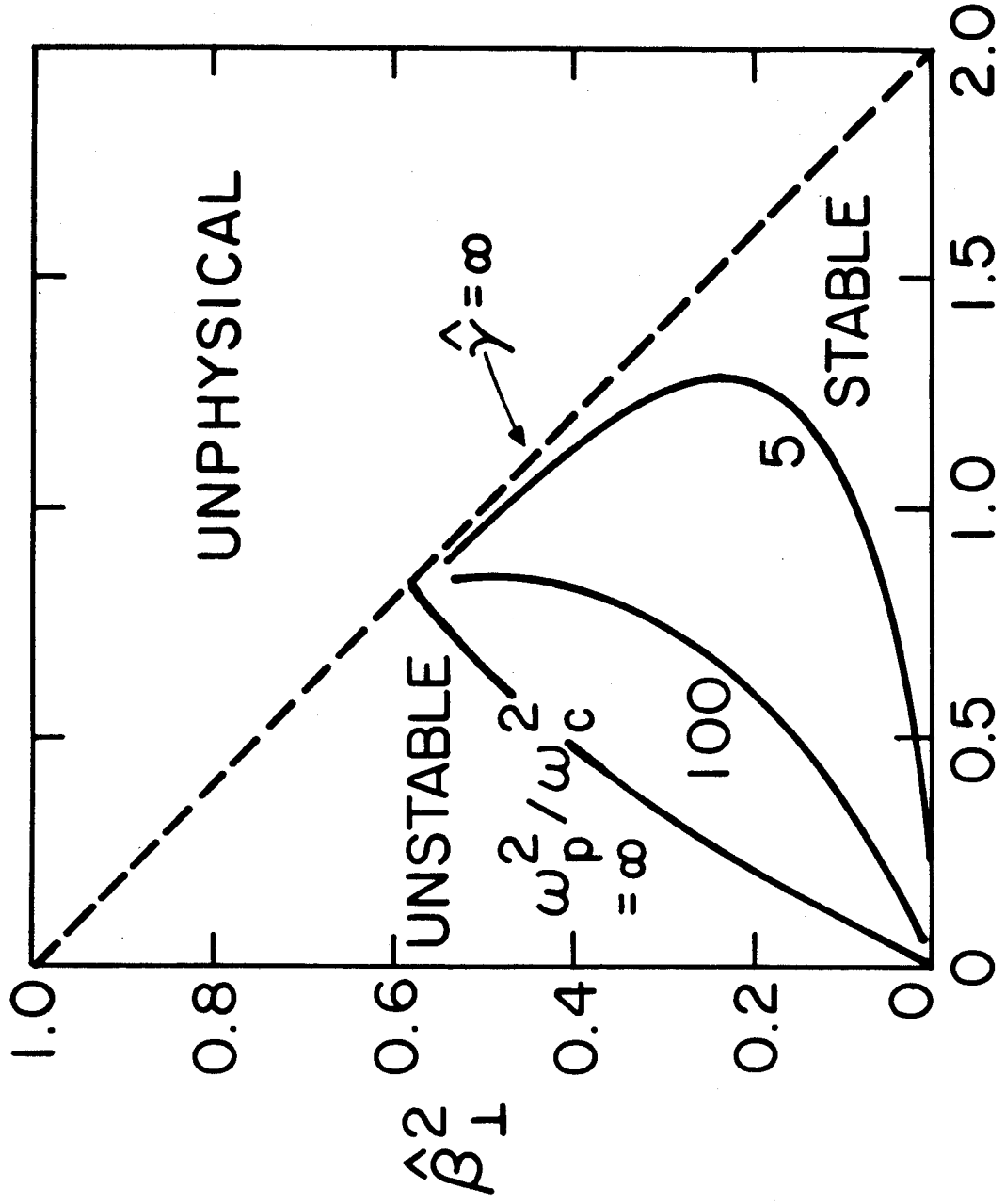
UNPHYSICAL
UNSTABLE
STABLE
$\hat{\gamma}=\infty$
$\omega_p^2/\omega_c^2 = \infty$
100
5
1.0
0.8
0.6
0.4
0.2
0
0
0.5
1.0
1.5
2.0
$\hat{\beta}_\perp^2$
$2\hat{\beta}_z^2$

Fig. 14

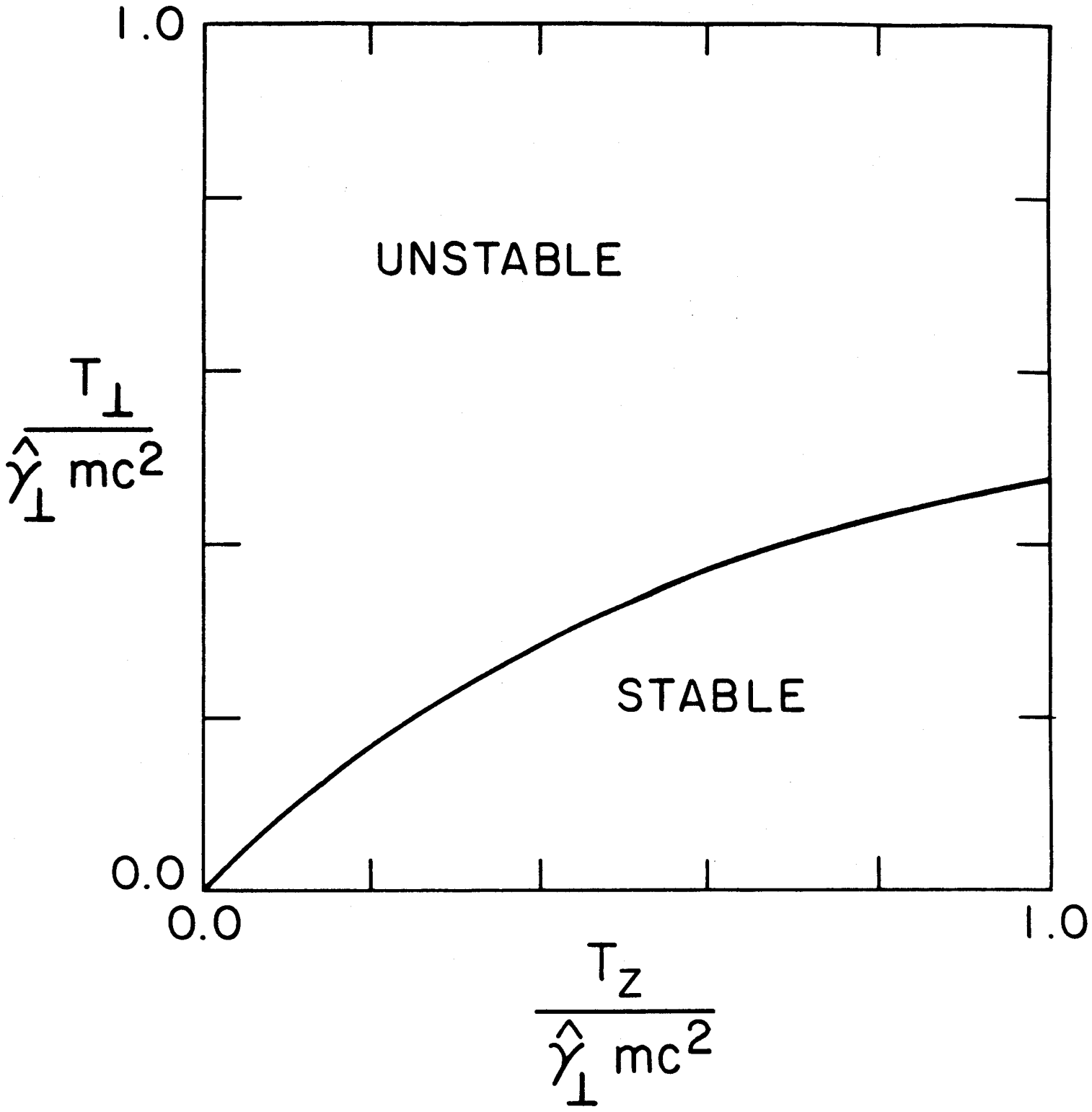
1.0
UNSTABLE
$\frac{T_\perp}{\hat{\gamma}_\perp mc^2}$
STABLE
0.0
0.0
1.0
$\frac{T_z}{\hat{\gamma}_\perp mc^2}$

Fig. 15